

1 **Constraining the sources of nitrogen fueling export  
2 production in the Gulf of Mexico using nitrogen isotope  
3 budgets**

4  
5 ANGELA N. KNAPP<sup>\*1</sup>, RACHEL K. THOMAS<sup>1</sup>, MICHAEL R. STUKEL<sup>1</sup>, THOMAS B. KELLY<sup>1</sup>, MICHAEL R.  
6 LANDRY<sup>2</sup>, KAREN E. SELPH<sup>3</sup>, ESTRELLA MALCA<sup>4,5</sup>, TRIKA GERARD<sup>5</sup>, JOHN LAMKIN<sup>5</sup>

7  
8 <sup>1</sup>EOAS Dept., Florida State University, Tallahassee, FL 32306, USA

9 <sup>2</sup>Scripps Inst. of Oceanography, University of California at San Diego, La Jolla, CA, 92093-0227, USA

10 <sup>3</sup>School of Ocean and Earth Science and Technology, Department of Oceanography, University of  
11 Hawai'i at Manoa, 1000 Pope Road, Honolulu, HI 96822, United States

12 <sup>4</sup>Cooperative Institute of Marine and Atmospheric Studies, University of Miami, Miami, FL, 33149  
13 USA

14 <sup>5</sup>Southeast Fisheries Science Center, NOAA National Marine Fisheries Service, Miami,  
15 FL, 33149 USA

16  
17 \*Corresponding author: [anknapp@fsu.edu](mailto:anknapp@fsu.edu)

18  
19 Keywords: Gulf of Mexico,  $\delta^{15}\text{N}$  budget, nitrate  $\delta^{15}\text{N}$ , regenerated production

22 **Abstract**

23  
24 The availability of nitrogen (N) in ocean surface waters affects rates of photosynthesis and marine  
25 ecosystem structure. In spite of low dissolved inorganic N concentrations, export production in  
26 oligotrophic waters is comparable to more nutrient replete regions. Prior observations raise the  
27 possibility that di-nitrogen (N<sub>2</sub>) fixation supplies a significant fraction of N supporting export  
28 production in the Gulf of Mexico. In this study, geochemical tools were used to quantify the relative  
29 and absolute importance of both subsurface nitrate and N<sub>2</sub> fixation as sources of new N fueling export  
30 production in the oligotrophic Gulf of Mexico in May 2017 and May 2018. Comparing the isotopic  
31 composition (“δ<sup>15</sup>N”) of nitrate with the δ<sup>15</sup>N of sinking particulate N indicates that N<sub>2</sub> fixation is  
32 typically not detected and that the majority ( $\geq 80\%$ ) of export production is supported by subsurface  
33 nitrate. Moreover, no gradients in upper ocean dissolved organic N and suspended particulate N  
34 concentration and/or δ<sup>15</sup>N were found that would indicate significant N<sub>2</sub> fixation fluxes accumulated in  
35 these pools, consistent with low *Trichodesmium* spp. abundance. Finally, comparing the δ<sup>15</sup>N of sinking  
36 particulate N captured within vs. below the euphotic zone indicates that regenerated N is low in δ<sup>15</sup>N  
37 compared to sinking N.

38  
39  
40 **Keywords: Gulf of Mexico, δ<sup>15</sup>N budget, nitrate δ<sup>15</sup>N, regenerated production**

43 **INTRODUCTION**

44 Primary productivity in the ocean accounts for roughly half of annual global carbon (C)  
45 fixation. Despite low concentrations of inorganic forms of nitrogen (N), such as nitrate ( $\text{NO}_3^-$ ) and  
46 ammonium ( $\text{NH}_4^+$ ), in many parts of the low-latitude surface ocean, significant rates of C fixation occur  
47 in these seemingly nutrient impoverished regions (Emerson, 2014). Phytoplankton carrying out this  
48 photosynthesis not only play a crucial role in the global C cycle, and thus impact climate, but create the  
49 foundation of the marine food web. Two sources of N that fuel “new” primary production are  $\text{NO}_3^-$ , the  
50 dominant bioavailable form of N in the global ocean, and biologically-mediated di-nitrogen ( $\text{N}_2$ )  
51 fixation (Dugdale & Goering, 1967). New production fueled by subsurface  $\text{NO}_3^-$  in mid- to high-  
52 latitude waters is supported by vertical mixing as thermocline stability erodes seasonally, with  $\text{N}_2$   
53 fixation thought to be more important in thermally stratified low-latitude surface waters. This “new”  
54 production is contrasted with photosynthesis supported by  $\text{NH}_4^+$ , known as “regenerated” production,  
55 that largely cycles in the surface ocean and does not contribute to export (Dugdale & Goering, 1967,  
56 Eppley & Peterson, 1979). While the distribution and rates of  $\text{N}_2$  fixation in the ocean play a central  
57 role in regulating the fertility and community structure of marine ecosystems, these first-order  
58 properties of marine  $\text{N}_2$  fixation remain poorly constrained. The highest short-term rates of  $\text{N}_2$  fixation  
59 have been documented in the tropical North Atlantic (Mahaffey *et al.*, 2005, Sohm *et al.*, 2011) as well  
60 as the western tropical South Pacific (Caffin *et al.*, 2018, Knapp *et al.*, 2018b). The spatial distribution  
61 of elevated  $^{15}\text{N}_2$  incubation-based  $\text{N}_2$  fixation rates (Luo *et al.*, 2012) are consistent with both the high  
62 preference of diazotrophs for warm waters (Breitbarth *et al.*, 2007, Stal, 2009) as well as the high  
63 atmospheric dust flux to the North Atlantic (Mahowald *et al.*, 2009, Prospero, 1996) that helps fulfill  
64 the significant iron requirement of the enzyme, nitrogenase, that catalyzes  $\text{N}_2$  fixation (Berman-Frank *et*  
65 *al.*, 2001, Kustka *et al.*, 2003). However, field observations are spatially limited, leaving modeling  
66 efforts to identify the regions of the global ocean supporting the largest  $\text{N}_2$  fixation fluxes under-  
67 constrained.

68 Both  $\text{N}_2$  fixation rates and fluxes of subsurface  $\text{NO}_3^-$  to surface waters are expected to respond  
69 to global change (Capotondi *et al.*, 2012, Luo *et al.*, 2019, Shi *et al.*, 2012), underscoring the  
70 importance of accurately characterizing their roles in supporting low-latitude C fixation. While  
71 incubation-based estimates of  $\text{NO}_3^-$  uptake and  $\text{N}_2$  fixation rates are commonly used to evaluate their  
72 respective roles in surface waters (Shiozaki *et al.*, 2018), these measurements have limitations,  
73 including potential bottle effects (Westberry *et al.*, 2012), the inherent short-term nature of the  
74 measurements, and challenges in consistently implementing methodological protocols (White *et al.*,  
75 2020). While incubation-based approaches are valuable, geochemical methods to evaluate  $\text{NO}_3^-$  vs.  $\text{N}_2$

fixation fueled export complement our understanding of this process. One geochemical tool to quantify relative and absolute contributions of subsurface  $\text{NO}_3^-$  and  $\text{N}_2$  fixation to export production relies on the distinct isotopic compositions ("δ<sup>15</sup>N") of these two N sources ("δ<sup>15</sup>N", where δ<sup>15</sup>N = {[<sup>15</sup>N/<sup>14</sup>N]<sub>sample</sub>/<sup>15</sup>N/<sup>14</sup>N]<sub>reference</sub>] - 1) \* 1000, with atmospheric  $\text{N}_2$  as the reference).  $\text{N}_2$  fixation introduces new N to the ocean with a δ<sup>15</sup>N of ~ -2 to 0‰ (Carpenter *et al.*, 1997, Hoering & Ford, 1960, Minagawa & Wada, 1986). In contrast, the δ<sup>15</sup>N of  $\text{NO}_3^-$  mixed up from the subsurface in the western North Atlantic can range from 2 to 4‰ (Knapp *et al.*, 2008, Knapp *et al.*, 2005, Marconi *et al.*, 2015). Assuming these are the dominant inputs of new N to the euphotic zone, in steady state, the δ<sup>15</sup>N of N fluxes out of the euphotic zone should reflect the relative importance of these N inputs. This "δ<sup>15</sup>N budget" approach assumes that sinking particulate N (PN<sub>sink</sub>) is the major flux of N out of the euphotic zone, and compares the δ<sup>15</sup>N of subsurface  $\text{NO}_3^-$  and  $\text{N}_2$  fixation with that of PN<sub>sink</sub>.

Given these assumptions, the relative importance of each source of new N for supporting export production can be estimated using the two end-member mixing model described in Eqn. 1, where the fractional importance of  $\text{N}_2$  fixation for supporting export production (x) is defined as:

$$\text{PN}_{\text{sink}} \delta^{15}\text{N} = x(-1\%) + (1 - x)(\text{NO}_3^- + \text{NO}_2^- \delta^{15}\text{N}) \quad \text{Eqn. 1}$$

Rearranging and solving for x yields:

$$x = (\text{NO}_3^- + \text{NO}_2^- \delta^{15}\text{N} - \text{PN}_{\text{sink}} \delta^{15}\text{N}) / (1 + \text{NO}_3^- + \text{NO}_2^- \delta^{15}\text{N}) \quad \text{Eqn. 2}$$

Multiplying "x" by the PN<sub>sink</sub> mass flux provides a time-integrated  $\text{N}_2$  fixation rate that can be compared with <sup>15</sup>N<sub>2</sub> incubation-based  $\text{N}_2$  fixation rate measurements (Knapp *et al.*, 2016a).

Prior δ<sup>15</sup>N budgets have been applied in oligotrophic waters like the Gulf of Mexico (GoM) where euphotic zone  $\text{NO}_3^-$  concentrations are low and  $\text{N}_2$  fixation is thought to potentially support a significant (i.e., >10%) fraction of export production. Although  $\text{N}_2$  fixation has recently been found to support the majority of export production at one location in the southwest Pacific Ocean (Knapp *et al.*, 2018b), and in the eastern North Atlantic  $\text{N}_2$  fixation has been found to support up to 40% of export (Bourbonnais *et al.*, 2009), even in regions where  $\text{N}_2$  fixation rates are relatively high, δ<sup>15</sup>N budgets indicate that subsurface  $\text{NO}_3^-$  fuels the majority of export production in the oligotrophic Atlantic and Pacific gyres (e.g., (Altabet, 1988, Casciotti *et al.*, 2008, Knapp *et al.*, 2016a, Knapp *et al.*, 2005)). Indeed, when δ<sup>15</sup>N budgets do indicate  $\text{N}_2$  fixation is a significant N source (Knapp *et al.*, 2018b), <sup>15</sup>N<sub>2</sub> uptake rates (Caffin *et al.*, 2018) and diazotroph abundance (Stenegren *et al.*, 2018) are notably elevated and consistent with diazotroph "bloom" conditions that fall outside typical <sup>15</sup>N<sub>2</sub> uptake

106 observations (Luo *et al.*, 2012), thus leaving a clear signature when N<sub>2</sub> fixation is a quantitatively  
107 important source of new N supporting export production.

108 Typical  $\delta^{15}\text{N}$  budget results appear consistent with related work indicating that not only is NO<sub>3</sub><sup>-</sup>  
109 the dominant new N input to low-latitude surface waters, but that its distinct isotopic composition  
110 propagates through geochemical N pools as well as the food web of oligotrophic gyres. At the base of  
111 the food web, this has been shown near Bermuda where, even during stratified summer conditions,  
112 eukaryotes consuming NO<sub>3</sub><sup>-</sup> are responsible for new production (Fawcett *et al.*, 2011). The importance  
113 of NO<sub>3</sub><sup>-</sup> as a N source to the low latitude ocean is also evident in the isotopic composition of dissolved  
114 organic nitrogen (DON). Phytoplankton release a fraction of new production as DON (Bronk & Ward,  
115 1999, Bronk & Ward, 2000, Bronk & Ward, 2005, Ward & Bronk, 2001). The distinct  $\delta^{15}\text{N}$  of surface  
116 ocean DON in the subtropical North Pacific versus the subtropical North Atlantic reflects the difference  
117 in  $\delta^{15}\text{N}$  of subsurface NO<sub>3</sub><sup>-</sup> of the two basins (Knapp *et al.*, 2011), again emphasizing the primary role  
118 of NO<sub>3</sub><sup>-</sup> in supporting low-latitude production. Similarly, the  $\delta^{15}\text{N}$  of suspended particulate N (PN<sub>susp</sub>)  
119 in the surface ocean, a fraction of which includes living phytoplankton, also exhibits variations that  
120 track regional differences in the  $\delta^{15}\text{N}$  of subsurface NO<sub>3</sub><sup>-</sup>. For example, surface ocean PN<sub>susp</sub>  $\delta^{15}\text{N}$   
121 ranges from 5 to 15‰ in regions with relatively high subsurface NO<sub>3</sub><sup>-</sup>  $\delta^{15}\text{N}$  such as in oxygen deficient  
122 zones (Knapp *et al.*, 2016a, White *et al.*, 2013). In contrast, the relatively low  $\delta^{15}\text{N}$  of PN<sub>susp</sub> in surface  
123 waters of the Sargasso Sea typically ranges from -1 to 0‰ (Altabet, 1988) and subsurface NO<sub>3</sub><sup>-</sup>  $\delta^{15}\text{N}$  is  
124 particularly low, 2 to 4‰ (Knapp *et al.*, 2008, Marconi *et al.*, 2017). Regional variations in subsurface  
125 NO<sub>3</sub><sup>-</sup>  $\delta^{15}\text{N}$  are also evident further up the food web in the  $\delta^{15}\text{N}$  of zooplankton biomass, which is higher  
126 in the North Pacific (Hannides *et al.*, 2009) than North Atlantic (McClelland *et al.*, 2003).

127 While results from prior  $\delta^{15}\text{N}$  budgets might lead to the expectation that subsurface NO<sub>3</sub><sup>-</sup> is the  
128 dominant source of new N to GoM surface waters, the same environmental conditions that are thought  
129 to support significant rates of N<sub>2</sub> fixation in the tropical North Atlantic are also commonly found in the  
130 GoM. Modest N<sub>2</sub> fixation rates, up to 2.3 nmol N L<sup>-1</sup> d<sup>-1</sup>, have been measured on the West Florida Shelf  
131 (Mulholland *et al.*, 2006, Mulholland *et al.*, 2014) and off of the northern GoM shelf, 85  $\mu\text{mol N m}^{-2} \text{ d}^{-1}$   
132 (Holl *et al.*, 2007), but the contribution of N<sub>2</sub> fixation to export production in the open waters of the  
133 GoM has not been quantified. Here we apply  $\delta^{15}\text{N}$  budgets to evaluate the relative importance of  
134 subsurface NO<sub>3</sub><sup>-</sup> and N<sub>2</sub> fixation for supporting export production in the oligotrophic GoM, as well as to  
135 estimate geochemically-derived rates of N<sub>2</sub> fixation. A novel addition to these  $\delta^{15}\text{N}$  budgets is the  
136 inclusion of estimates of zooplankton NH<sub>4</sub><sup>+</sup> and/or urea excretion as a secondary mechanism of N  
137 export from the euphotic zone.

138 **METHODS**139 **Sample collection**

140 Samples were collected for inorganic nutrient concentration and isotopic analysis on the NOAA  
141 Ship *Nancy Foster* from May 11-29 of 2017 (“NF1704”) and April 30 to May 19 of 2018 (“NF1802”)  
142 in the deep waters of the northern and central GoM (Fig. 1). Samples were also collected for DON  
143 concentration and isotopic analysis on the NF1802 cruise. Details of the cruises can be found in (Gerard  
144 *et al.*, In Review). Briefly, samples were collected during five Lagrangian experiments of two- to four-  
145 day duration (i.e. “cycles”), each initiated with the deployment of free-drifting, mixed-layer-drogued  
146 sediment traps and concluded with their recovery. The length of trap deployment was chosen to  
147 accommodate multiple cycles per cruise, with longer cycles conducted where patches of bluefin tuna  
148 larvae were observed. Cycles over the course of the two cruises were sequentially numbered, with the  
149 first three cycles on the 2017 cruise referenced as NF1704-C1 (C1), NF1704-C2 (C2), and NF1704-C3  
150 (C3), and the two cycles on the 2018 cruise referenced as NF1802-C4 (C4), and NF1802-C5 (C5).  
151 During the Lagrangian experiments, water-column samples were collected from Niskin bottles  
152 deployed on a CTD-rosette close to the drifting sediment trap array at ~0200 local time each day.  
153 Nutrient samples were collected in the dark to accommodate pre-dawn sampling for light incubation  
154 experiments (Yingling *et al.*, 2021). Nutrient samples passed an acid-cleaned 0.2- $\mu$ m membrane filter  
155 and were stored frozen at -20 °C in acid-washed HDPE bottles for analysis on land, per GEOTRACES  
156 protocols (Cutter *et al.*, 2014). The depth of the mixed layer, defined as the depth at which density  
157 increased by 0.125 kg m<sup>-3</sup> (Monterey & Levitus, 1997), ranged from 21-36 m during NF1704 (C1-C3)  
158 and 11-27 m during NF1802 (C4-C5).

159  
160 **NO<sub>3</sub><sup>-</sup>+NO<sub>2</sub><sup>-</sup>, ammonium, phosphate, and DON concentrations**

161 The concentrations of NO<sub>3</sub><sup>-</sup>+nitrite (NO<sub>3</sub><sup>-</sup>+NO<sub>2</sub><sup>-</sup>) in water-column samples were measured using  
162 a chemiluminescent method with a lower quantification limit of 0.1  $\mu$ M and mean standard deviation of  
163  $\pm$ 0.1  $\mu$ M (Braman & Hendrix, 1989). Concentrations of NH<sub>4</sub><sup>+</sup> were quantified using the fluorescent  
164 OPA method with a lower limit of 25 nM and mean standard deviation of  $\pm$ 20 nM (Holmes *et al.*,  
165 1999). Soluble reactive phosphorus (PO<sub>4</sub><sup>3-</sup>) concentration measurements were made using colorimetric  
166 methods with a lower quantification limit of 50 nM (Koroleff, 1983). Concentrations of total dissolved  
167 nitrogen (TDN) were measured using persulfate oxidation of TDN to NO<sub>3</sub><sup>-</sup> according to (Knapp *et al.*,  
168 2005), and the resulting NO<sub>3</sub><sup>-</sup> concentration was measured using chemiluminescence as described  
169 above. The concentration of DON was calculated by subtracting the concentrations of NO<sub>3</sub><sup>-</sup>+NO<sub>2</sub><sup>-</sup> and

170 NH<sub>4</sub><sup>+</sup> from the TDN concentration. In samples with undetectable levels of NO<sub>3</sub><sup>-</sup>+NO<sub>2</sub><sup>-</sup> (i.e., most  
171 samples in the upper 100 m), the average standard deviation of DON concentration was  $\pm 0.3$   $\mu\text{M}$ , with  
172 a propagated error for DON concentration with detectable levels of NO<sub>3</sub><sup>-</sup>+NO<sub>2</sub><sup>-</sup> of  $\pm 0.32$   $\mu\text{M}$ .

173

174 **NO<sub>3</sub><sup>-</sup>+NO<sub>2</sub><sup>-</sup>  $\delta^{15}\text{N}$ ,  $\delta^{18}\text{O}$  and DON  $\delta^{15}\text{N}$  measurements**

175 The  $\delta^{15}\text{N}$  of NO<sub>3</sub><sup>-</sup>+NO<sub>2</sub><sup>-</sup> in samples was measured using the denitrifier method (Casciotti *et al.*,  
176 2002, Sigman *et al.*, 2001, Weigand *et al.*, 2016) and calibrated using standard bracketing techniques  
177 with IAEA N3 ( $\delta^{15}\text{N} = 4.7\text{\textperthousand}$ ,  $\delta^{18}\text{O} = 25.6\text{\textperthousand}$ ), and USGS 34 ( $\delta^{15}\text{N} = -1.8\text{\textperthousand}$ ,  $\delta^{18}\text{O} = -27.9\text{\textperthousand}$ ), and for  
178  $\delta^{18}\text{O}$ , additionally with USGS 35 ( $\delta^{18}\text{O} = 57.5\text{\textperthousand}$ ) as described by (Mcilvin & Casciotti, 2011). The  
179 mean standard deviation of replicate NO<sub>3</sub><sup>-</sup>+NO<sub>2</sub><sup>-</sup>  $\delta^{15}\text{N}$  and  $\delta^{18}\text{O}$  analyses was  $\leq 0.2\text{\textperthousand}$ . The  $\delta^{15}\text{N}$  of TDN  
180 was determined using persulfate oxidation according to (Knapp *et al.*, 2005), with the resulting NO<sub>3</sub><sup>-</sup>  
181 determined with the denitrifier method after adjusting the sample to pH=4. The  $\delta^{15}\text{N}$  of DON was  
182 calculated by mass balance by subtracting the concentration and  $\delta^{15}\text{N}$  of NO<sub>3</sub><sup>-</sup>+NO<sub>2</sub><sup>-</sup> from the TDN  
183 concentration and  $\delta^{15}\text{N}$ . When the concentration of NO<sub>3</sub><sup>-</sup>+NO<sub>2</sub><sup>-</sup> was below detection, the average  
184 standard deviation of duplicate analyses of DON  $\delta^{15}\text{N}$  was  $\pm 0.3\text{\textperthousand}$ . When the concentration of NO<sub>3</sub><sup>-</sup>  
185 +NO<sub>2</sub><sup>-</sup> was proportionate to the concentration of DON in the sample the propagated error for replicate  
186 analyses of DON  $\delta^{15}\text{N}$  was  $\pm 0.6\text{\textperthousand}$ , determined using a Monte Carlo approach (Press *et al.*, 1992).

187

188 **Chlorophyll *a* concentration, *Trichodesmium* spp. abundance, and suspended particulate N  
189 concentration and  $\delta^{15}\text{N}$  measurements**

190 The concentration of chlorophyll *a* was determined by calibrating the CTD fluorescence sensor  
191 with Niskin-bottle based HPLC pigments as described in Selph *et al.* (2021). Additionally, trichomes of  
192 the diazotroph *Trichodesmium* spp. were enumerated digitally using an OMAX A355OU camera and  
193 TouPLite software as described in (Selph *et al.*, 2021). Suspended particulate organic nitrogen (PN<sub>susp</sub>)  
194 was collected by filtering 2.2 L of water onto a pre-combusted (450 °C for 4 h) Whatman glass fiber  
195 filter and its mass and isotopic composition was determined by an elemental analyzer interfaced to an  
196 isotope ratio mass spectrometer at the UC Davis Stable Isotope Facility with a lower detection limit of  
197 2.2  $\mu\text{g N}$  and precision of  $\pm 0.3\text{\textperthousand}$  for 80  $\mu\text{g N}$  samples.

198

199 **Sinking particulate N flux and  $\delta^{15}\text{N}$  measurements**

200       Surface-tethered, VERTEX-style particle-interceptor traps (PIT) were deployed at three depths: a  
201       “shallow” trap deployed at 60 m, below the mixed layer; a “mid-depth” trap deployed just below the  
202       base of the euphotic zone (i.e., 117 m on C5, 140 m on C1-C3, and 151 m on C4); and a “deep” trap  
203       deployed at 231 m. PIT tubes (8:1 aspect ratio, baffle on top constructed of smaller tubes with 8:1  
204       aspect ratio) were deployed with a formalin-brine for 2.2 to 4.5 days. After recovery, they were filtered  
205       through a 100- $\mu$ m filter and swimmers were removed during inspection at 25X magnification (Zeiss  
206       stereomicroscope). Triplicate brine tubes were then filtered through pre-combusted Whatman glass  
207       fiber filters and the N mass flux (“ $PN_{sink}$  flux”) and  $\delta^{15}\text{N}$  of the  $PN_{sink}$  flux were determined as  
208       described above for suspended particles. A complete description of the sediment trap deployment and  
209       sample collection is given in (Stukel *et al.*, 2021).

210

## 211       **Zooplankton excretion flux and its isotopic composition**

212       Estimates of N loss from the euphotic zone due to excretion of diel migrant zooplankton at their  
213       mesopelagic daytime depths were calculated from the size-fractioned biomass measurements of  
214       (Landry & Swalethorp, 2021) and the empirical allometric relationship of Ikeda (1985) for ammonium  
215       and/or urea excretion (E:  $\mu\text{g N organism}^{-1} \text{ h}^{-1}$ ):

$$216 \quad \ln E = -2.176 + 0.829 \ln C_i + 0.0648 T$$

217       where  $C_i$  is the average carbon content of individual zooplankters in size fraction  $i$  and  $T$  ( $^{\circ}\text{C}$ ) is the  
218       environmental temperature at 300-500 m. Mesozooplankton were collected daily during experimental  
219       cycles at mid-day and mid-night with a 1-m diameter ring net (0.2-mm Nitex mesh) towed obliquely  
220       through the euphotic zone. The collected organisms were wet sieved through nested Nitex screens of 5,  
221       2, 1, 0.5 and 0.2 mm Nitex mesh to produce 5 size classes of 0.2-0.5, 0.5-1, 1-2, 2-5 and  $>5$  mm. Size  
222       fractions were oven dried ( $60^{\circ}\text{C}$ ) for total dry weight, ground to a powder, and analyzed for C and N  
223       content and isotopes ( $\delta^{13}\text{C}$  and  $\delta^{15}\text{N}$ ) by an elemental analyzer coupled to an isotope ratio mass  
224       spectrometer (EA-IRMS) (Owens and Rees, 1989). For each pair of day-night samples, migrant  
225       biomass was determined as the difference between night-day carbon for each size fraction. For  
226       individual carbon contents,  $C_i$ , in the Ikeda (1985) equation, we used mean values of 2.4, 7.4, 41, 140  
227       and  $2782 \mu\text{g C ind}^{-1}$  for the 0.2-0.5 to  $>5$  mm size fractions, respectively (Landry *et al.*, 2001). Migrant  
228       abundances in each size fraction were calculated from measured C biomass and the individual  $C_i$   
229       estimates, and migrants were assumed to spend  $12 \text{ h d}^{-1}$  at mesopelagic depths (300-500 m).

230       Since few have measured it directly, we consider the  $\delta^{15}\text{N}$  of zooplankton excretion to be  
231       relatively uncertain. Consequently, we used lower and upper bound estimates, 3‰ and 5‰,

232 respectively, for the magnitude of the isotope effect associated with zooplankton N excretion. The 3‰  
233 estimate reflects the difference between the  $\delta^{15}\text{N}$  of copepod and doliolid biomass and excreted N in the  
234 northwest Pacific Ocean (Checkley & Miller, 1989). This estimate is also consistent with prior studies  
235 of N isotopic enrichment in food webs (Checkley & Entzeroth, 1985, Deniro & Epstein, 1981,  
236 Minagawa & Wada, 1984, Wada *et al.*, 1987). The 5‰ estimate comes from organismal N mass and  
237 isotopic observational and modeling constraints (Stukel *et al.*, 2018). Uncertainties in the day-night  
238 biomass of each size class were propagated through all measurements using Monte Carlo approaches.  
239

## 240 RESULTS

### 241 $\text{NO}_3^- + \text{NO}_2^-$ concentration, $\delta^{15}\text{N}$ , $\delta^{18}\text{O}$

242 The concentration of  $\text{NO}_3^- + \text{NO}_2^-$  in the upper 100 m was  $\leq 0.1 \mu\text{M}$  and increased with depth  
243 (Figs. 2 and 3). Water-column profiles of thermocline  $\text{NO}_3^- + \text{NO}_2^- \delta^{15}\text{N}$  and  $\delta^{18}\text{O}$  show similar trends  
244 among the cycles and little variation on potential density surfaces, with a  $\text{NO}_3^- + \text{NO}_2^- \delta^{15}\text{N}$  maximum of  
245 ~5‰ at 650 m, which decreases up through the shallower thermocline to a minimum of 2.0 to 3.0‰ at  
246 231 m (Figs. 2 and 3). The  $\delta^{18}\text{O}$  of  $\text{NO}_3^- + \text{NO}_2^-$  throughout the water column was largely  $1.5 \pm 0.5\text{‰}$   
247 (Fig. 3), with the  $\delta^{18}\text{O}$  of  $\text{NO}_3^- + \text{NO}_2^-$  in samples shallower than 150 m  $> 3.0\text{‰}$  in the same samples with  
248 elevated  $\text{NO}_3^- + \text{NO}_2^- \delta^{15}\text{N}$  (Fig. 3).

249

### 250 DON and $\text{PN}_{\text{susp}}$ concentration and $\delta^{15}\text{N}$

251 DON concentration in the NF1802 samples was largely consistent among stations (Fig. 4).  
252 Profile concentrations averaged between 4 and 5  $\mu\text{M}$  in the upper 100 m. The mean  $\delta^{15}\text{N}$  of DON  
253 varied between 3.0 and 3.5‰, but showed more variability among stations than DON concentration  
254 (Figs. 4 and 5). Exceptions to these mean values include a station from C5 near the shelf/slope break  
255 where higher DON concentration (7.3  $\mu\text{M}$ ) was found in surface waters with a relatively elevated  $\delta^{15}\text{N}$   
256 of 4.5‰ (Fig. 4). This surface water sample also had a relatively low salinity (35.28) compared with the  
257 underlying 40 m sample (36.45). However, other samples further offshore with a similar salinity, 35.0  
258 to 36.0, had a  $\delta^{15}\text{N}$  between 3.0 and 4.0‰ (Fig. 4). Other samples near the shelf/slope break collected  
259 from 75 and 100 m with relatively high DON  $\delta^{15}\text{N}$ , from 4.0 to 6.0‰, had salinities  $> 36$ . Additionally,  
260 two stations further offshore had  $\delta^{15}\text{N}$  DON  $< 3\text{‰}$  at several depths in the upper 100 m (Fig. 4). All

samples at these stations had salinity >36. No significant changes in DON concentration or  $\delta^{15}\text{N}$  were found over the course of the Lagrangian cycles (Figs. 4 and 5).

The mean  $\text{PN}_{\text{susp}}$  concentration in the upper 100 m on the NF1704 cruise was  $\sim 1.0 \mu\text{M}$ , and ranged from 0.7 to  $2.0 \mu\text{M}$  and was higher than the mean  $\text{PN}_{\text{susp}}$  concentration on the NF1802 cruise (mean  $\sim 0.6 \mu\text{M}$ , ranging from 0.3 to  $1.3 \mu\text{M}$ ) (Fig. 5) (Table III). The mean  $\delta^{15}\text{N}$  of  $\text{PN}_{\text{susp}}$  on NF1704, 1.0 to  $2.0\text{\textperthousand}$ , was not significantly different from that on NF1802, 1.0 to  $2.5\text{\textperthousand}$ . Finally, like DON, we found no significant gradients with depth or over the course of the Lagrangian cycles for either  $\text{PN}_{\text{susp}}$  concentration or  $\delta^{15}\text{N}$  in the upper 100 m (Fig. 5) (Table III).

## The flux and isotopic composition of $\text{PN}_{\text{sink}}$ and zooplankton excretion

The largest flux of N out of the euphotic zone was the  $\text{PN}_{\text{sink}}$  flux. The range and mean  $\text{PN}_{\text{sink}}$  mass flux ( $\pm 1 \text{ S.D.}$ ) and mean, mass-weighted  $\delta^{15}\text{N}$  of the  $\text{PN}_{\text{sink}}$  flux ( $\pm 1 \text{ S.D.}$ ) for each cycle, determined by averaging the  $\text{PN}_{\text{sink}}$  collected in three brine tubes per floating sediment trap deployment, is reported in Table I (Fig. 2). The mean  $\text{PN}_{\text{sink}}$  mass flux into the 60 m traps, representing upper euphotic zone export from the mixed layer, ranged from  $0.59 \pm 0.04$  (C4) to  $1.53 \pm 0.6$  (C1)  $\text{mmol N m}^{-2} \text{ d}^{-1}$  (Table I). Mean  $\text{PN}_{\text{sink}}$  fluxes out of the euphotic zone, as recorded by the mid-depth trap, ranged from  $0.46 \pm 0.02$  (C1) to  $1.1 \pm 0.18$  (C3)  $\text{mmol N m}^{-2} \text{ d}^{-1}$  (Table I). The mean  $\text{PN}_{\text{sink}}$  mass flux decreased with depth except for C3, when the  $\text{PN}_{\text{sink}}$  flux in the 140 m trap was larger than (although not significantly different from) that captured in the 60 m trap,  $1.1 \pm 0.18$  vs.  $0.98 \pm 0.26 \text{ mmol N m}^{-2} \text{ d}^{-1}$ , respectively (Table I). The  $\text{PN}_{\text{sink}}$  flux in the 231 m trap was 35 to 50% of the  $\text{PN}_{\text{sink}}$  flux at the base of the euphotic zone (Table I). The mean  $\delta^{15}\text{N}$  of the  $\text{PN}_{\text{sink}}$  flux at 60 m, ranging from  $1.6 \pm 0.3\text{\textperthousand}$  (C3) to  $3.8 \pm 0.2\text{\textperthousand}$  (C5), was lower than the  $\delta^{15}\text{N}$  of  $\text{PN}_{\text{sink}}$  flux in the deeper traps (Fig. 2, Table I). The  $\delta^{15}\text{N}$  of the  $\text{PN}_{\text{sink}}$  flux in the deepest two traps were typically more similar to each other than the  $\delta^{15}\text{N}$  of the  $\text{PN}_{\text{sink}}$  flux in the euphotic zone, and the mean  $\delta^{15}\text{N}$  for both of the deeper traps ranged from  $2.9 \pm 0.1\text{\textperthousand}$  (C2, 120 m) to  $5.0 \pm 0.2\text{\textperthousand}$  (C5, 231 m) (Table I). Finally, we note that the  $\delta^{15}\text{N}$  of the  $\text{PN}_{\text{sink}}$  flux was always higher than the  $\delta^{15}\text{N}$  of  $\text{PN}_{\text{susp}}$ .

Since we observed no gradients either with depth or over the course of Lagrangian sampling in either  $\text{PN}_{\text{susp}}$  or DON concentration in the euphotic zone (Table III, Figs. 4 and 5), the only other quantifiable pathway for N loss from the euphotic zone is via excretion or defecation of nitrogenous waste from vertically migrating zooplankton at depth or mortality of these organisms at their daytime resting depths. The estimated rates of zooplankton N excretion, in the form of  $\text{NH}_4^+$  (Checkley & Miller, 1989) and urea (Bidigare, 1983), below the euphotic zone are reported in Table II. The mean

293 excretion rates of all vertically migrating zooplankton size classes were summed for each cycle, and  
294 range from  $19.6 \pm 49.1$  (C1) to  $171.7 \pm 103.3$  (C5)  $\mu\text{mol N m}^{-2} \text{d}^{-1}$  (Table II), with detailed descriptions  
295 of these fluxes in (Landry & Swalethorp, 2021). These zooplankton excretion fluxes are roughly an  
296 order of magnitude smaller than the  $\text{PN}_{\text{sink}}$  fluxes below the euphotic zone (Tables I and II). Although  
297 we could not quantify zooplankton mortality or defecation at depth, we believe these fluxes are also  
298 small relative to  $\text{PN}_{\text{sink}}$  and hence neglect them in further calculations. Estimates of the  $\delta^{15}\text{N}$  of  
299 zooplankton excretion assuming a 3‰ isotope effect range from 0.6 to 3.1‰ and are similar to or lower  
300 than the  $\delta^{15}\text{N}$  of both subsurface  $\text{NO}_3^- + \text{NO}_2^-$  and the  $\text{PN}_{\text{sink}}$  flux (Table I), which range from -0.8 to  
301 1.7‰ using the 5‰ isotope effect (Table II).

302

## 303 DISCUSSION

### 304 Comparison with prior regional observations

305 Water column profiles of  $\text{NO}_3^- + \text{NO}_2^-$  concentration and isotopic composition from these cruises  
306 were consistent with prior regional observations (Howe *et al.*, 2020). In particular, the decreasing  $\text{NO}_3^-$   
307 +  $\text{NO}_2^- \delta^{15}\text{N}$  up through the thermocline (Fig. 3) has been observed previously in the GoM and North  
308 Atlantic and is consistent with prior characterizations of the isotopic composition of  $\text{NO}_3^- + \text{NO}_2^-$  in  
309 regional water masses including the GoM (Howe *et al.*, 2020), the Florida Straits (Leichter *et al.*,  
310 2007), and the North Atlantic (Knapp *et al.*, 2008, Marconi *et al.*, 2015, Marconi *et al.*, 2019). The  
311 increasing  $\delta^{15}\text{N}$  and  $\delta^{18}\text{O}$  of  $\text{NO}_3^- + \text{NO}_2^-$  in the upper 150 m is consistent with  $\text{NO}_3^-$  assimilation at the  
312 base of the euphotic zone as has been observed previously in the region (Howe *et al.*, 2020, Knapp *et*  
313 *al.*, 2005). The similarities of GoM samples to  $\text{NO}_3^- + \text{NO}_2^-$  concentration,  $\delta^{15}\text{N}$ , and  $\delta^{18}\text{O}$  from the  
314 North Atlantic are consistent with the Loop Current importing thermocline water from the tropical and  
315 subtropical North Atlantic into the GoM (Hernandez-Guerra & Joyce, 2000, Hofmann & Worley, 1986,  
316 Morrison *et al.*, 1983, Wilson & Johns, 1997), as well as the relatively short residence time of water in  
317 the GoM (Amon *et al.*, 2020). The latter prevents N inputs from the Mississippi River, submarine  
318 groundwater discharge, and  $\text{N}_2$  fixation from significantly modifying the concentration and isotopic  
319 composition of  $\text{NO}_3^- + \text{NO}_2^-$  before leaving the GoM (Howe *et al.*, 2020).

320 To the best of our knowledge, these measurements of DON  $\delta^{15}\text{N}$  are the first reported from the  
321 GoM. As was found for the concentration and isotopic composition of  $\text{NO}_3^- + \text{NO}_2^-$ , these DON  
322 observations are consistent with regional observations from the Sargasso Sea, between 3.0 and 4.0‰  
323 (Figs. 4, 5) (Knapp *et al.*, 2005, Knapp *et al.*, 2011). The sample from C5 near the shelf/slope break  
324 with elevated DON concentration and  $\delta^{15}\text{N}$  and slightly lower salinity was collected near DeSoto

325 Canyon, and it is possible that the surface sample included freshwater DON, possibly from the  
326 Mississippi-Atchafalaya River System, other riverine (e.g., Apalachicola) inputs, benthic DON, and/or  
327 submarine groundwater discharge (Morey *et al.*, 2003). Alternatively, the elevated concentration and  
328 isotopic composition may reflect production of DON near the shelf/slope break (Kelly *et al.*, 2021) that  
329 underwent subsequent consumption with isotopic fractionation (Knapp *et al.*, 2018a, Zhang *et al.*,  
330 2020). Other samples collected near the shelf/slope break with elevated DON  $\delta^{15}\text{N}$  values deeper in the  
331 water column are not associated with a decrease in DON concentration between the surface and  
332 subsurface, indicating a different DON source and not remineralization with depth as a likely  
333 explanation with benthic sources potentially including submarine groundwater discharge (Sanial *et al.*,  
334 2021). A distinct DON source, such as benthic organic matter and/or submarine groundwater discharge,  
335 may also be responsible for the low- $\delta^{15}\text{N}$  DON (1.7‰) observed near De Soto Canyon (Fig. 4).

336 While 100 m samples collected offshore with relatively low DON  $\delta^{15}\text{N}$  (<3‰) and salinity >36  
337 were not associated with elevated *Trichodesmium* spp. trichome abundance, they may reflect recent  
338 low- $\delta^{15}\text{N}$  inputs not captured by *Trichodesmium* spp. abundance at the time of sampling. It is also  
339 notable that while *Trichodesmium* spp. were most abundant in the upper 20 m (Fig. 5) (Selph *et al.*,  
340 2021), consistent with prior observations of their depth distribution (Capone *et al.*, 2005), the  $\delta^{15}\text{N}$  of  
341 DON was not significantly lower in the upper 20 m than throughout the upper 100 m (Figs. 4 and 5).  
342 Thus, if DON was released by *Trichodesmium* spp., it did not accumulate to detectable levels in this  
343 pool (Knapp *et al.*, 2011), but instead may have been assimilated by other phytoplankton that could  
344 then contribute to the sinking flux (e.g., (Bonnet *et al.*, 2016, Knapp *et al.*, 2016b)). We note that  
345 *Trichodesmium* spp. trichome abundance was low compared to prior work in the Atlantic, where an  
346 average of >2000 trichomes L<sup>-1</sup> was observed (Carpenter *et al.*, 2004). No significant trends in DON  
347 concentration or  $\delta^{15}\text{N}$  with depth were observed, which is also consistent with losses of DON not  
348 typically observed in the upper 100 m in oligotrophic regions, but instead seen at or below 150 m  
349 (Knapp *et al.*, 2011). Finally, there is no evidence for differences in DON concentration in the upper 50  
350 m vs. the 50 to 100 m depth horizons (Figs. 4 and 5), as would be consistent with DON consumption  
351 within the euphotic zone observed in regions transitional between productive and oligotrophic regions  
352 (Knapp *et al.*, 2018a, Zhang *et al.*, 2020).

353 The mean PN<sub>susp</sub> concentration on these cruises, in particular on the NF1704 cruise, was higher  
354 than is typically found in oligotrophic environments such as Bermuda and Hawaii. The concentrations  
355 of PN<sub>susp</sub> on NF1802 were closer to those typically observed in oligotrophic euphotic zones such as  
356 near Hawaii and Bermuda, where PN<sub>susp</sub> concentrations are typically 0.3 to 0.4  $\mu\text{M}$  (Altabet, 1988,

357 Fujiki *et al.*, 2011). It is not clear why the PN<sub>susp</sub> was twice as high on NF1704 compared to NF1802, as  
358 chlorophyll *a* concentrations in the upper 50 m were not meaningfully different between the two years  
359 (Fig. 5), nor were other productivity metrics (Yingling *et al.*, 2021). The similarity of the mean  $\delta^{15}\text{N}$  of  
360 PN<sub>susp</sub> on both cruises suggests similar N supply and cycling mechanisms were at work during both  
361 cruises. Regardless, the  $\delta^{15}\text{N}$  of this PN<sub>susp</sub> was higher than that typically observed in the Sargasso Sea,  
362 -1 to 0‰ (Altabet, 1988, Fawcett *et al.*, 2011), or in other tropical Atlantic regions where diazotrophs  
363 are abundant (Montoya *et al.*, 2002).

364 The PN<sub>sink</sub> mass fluxes captured in the sub-euphotic zone traps are somewhat lower than  
365 observations closer to the northern Gulf of Mexico shelf/slope break region (Hung *et al.*, 2004; Hung *et*  
366 *al.*, 2010), but similar to other observations from the Gulf from deeper waters (Maiti *et al.*, 2014).  
367 Additionally, these PN<sub>sink</sub> fluxes are similar to results from the Sargasso Sea (Altabet, 1988) and are  
368 somewhat higher than fluxes in the oligotrophic North (Casciotti *et al.*, 2008, Christian *et al.*, 1997) and  
369 South Pacific (Knapp *et al.*, 2016a). Finally, the elevation of the  $\delta^{15}\text{N}$  of the PN<sub>sink</sub> flux relative to the  
370  $\delta^{15}\text{N}$  of PN<sub>susp</sub> is consistent with prior observations (Altabet, 1988, Altabet *et al.*, 1991, White *et al.*,  
371 2013).

### 373 **$\delta^{15}\text{N}$ budget constraints on the sources of N fueling export production in the GoM**

374 In spite of low inorganic nutrient concentrations, oligotrophic surface waters still support rates  
375 of export production comparable to regions with higher surface nutrient concentrations (Emerson,  
376 2014). Older  $\delta^{15}\text{N}$  budgets in a similarly stratified oligotrophic region near Hawaii have suggested that  
377 N<sub>2</sub> fixation provides as much as 50% of the N supporting export production (Karl *et al.*, 1997; Dore *et*  
378 *al.*, 2002). However, more recent  $\delta^{15}\text{N}$  budgets, employing sensitive methods to measure the  $\delta^{15}\text{N}$  of  
379 NO<sub>3</sub><sup>-</sup> present at lower concentrations immediately below the euphotic zone indicate that export  
380 production is primarily fueled by NO<sub>3</sub><sup>-</sup> near Hawaii (Casciotti *et al.*, 2008), assuming that the PN<sub>sink</sub>  
381 flux is the primary N loss pathway from the euphotic zone. Even though PN<sub>sink</sub> is the largest flux of N  
382 out of the euphotic zone, zooplankton vertical migration and mortality or N excretion at depth and  
383 vertical mixing of DOM and/or POM can also be an important vector for C and N loss from surface  
384 waters (Emerson, 2014) (Fig. 6). In the Sargasso Sea near Bermuda, previous  $\delta^{15}\text{N}$  budgets have  
385 considered the potential importance of DON and PN<sub>susp</sub> consumption as a N source fueling export  
386 production (Knapp *et al.*, 2005). In this previous study, with DON concentration and  $\delta^{15}\text{N}$  similar to  
387 those in the GoM, calculated DON and PN<sub>susp</sub> consumption did not play a quantitatively important role  
388 supporting export (Knapp *et al.*, 2005). Since a stably stratified water column suggested weak mixing

389 and DON and  $\text{PN}_{\text{susp}}$  vertical gradients were not pronounced (Table III, Figs. 4 and 5), and since no  
390 significant gradients were observed over the duration of the Lagrangian cycles either, we cannot  
391 include  $\text{PN}_{\text{susp}}$  or DON in these  $\delta^{15}\text{N}$  budget calculations. However, we note that consumption of either  
392  $\text{PN}_{\text{susp}}$  or DON at rates sufficient to support the magnitude of export production observed in the mid-  
393 depth trap would be difficult to resolve in these measurements. For instance, if the  $\text{PN}_{\text{sink}}$  flux in the  
394 sub-euphotic trap of C1,  $0.46 \text{ mmol N m}^{-2} \text{ d}^{-1}$  (Table I) was entirely supported by the consumption of  
395 DON or  $\text{PN}_{\text{susp}}$  occurring equally throughout the upper 100 m, it would correspond to a loss of  $4.6 \text{ nM}$   
396  $\text{N d}^{-1}$  from the DON or  $\text{PN}_{\text{susp}}$  pool, not detectable in these concentration measurements over the course  
397 of the 2-4 day cycles.

398 With the exception of a recent study (Stukel *et al.*, 2018), previous  $\delta^{15}\text{N}$  budgets have not  
399 quantified zooplankton N excretion at depth as another N loss term. Here, we include zooplankton  
400 excretion below the euphotic zone with the  $\text{PN}_{\text{sink}}$  flux in Eqn. 1 to estimate the  $\delta^{15}\text{N}$  of total N loss  
401 from the euphotic zone and compare that with the  $\delta^{15}\text{N}$  of the presumed largest source of N fueling  
402 export, subsurface  $\text{NO}_3^-$ ; Fig. 6 illustrates this conceptually and includes the  $\delta^{15}\text{N}$  of N pools and fluxes  
403 in this study. If the  $\delta^{15}\text{N}$  of the combined, mass-weighted N loss terms is lower than the  $\delta^{15}\text{N}$  of  
404 subsurface  $\text{NO}_3^-$  it implies that the  $\delta^{15}\text{N}$  budget is imbalanced and an additional source of N to the  
405 euphotic zone with a lower  $\delta^{15}\text{N}$  is required to balance the isotopic composition of N losses. Here, we  
406 assume  $\text{N}_2$  fixation is the best candidate for that low- $\delta^{15}\text{N}$  N source, which introduces N with a  $\delta^{15}\text{N}$   
407 between -2 and 0‰ to the euphotic zone (Carpenter *et al.*, 1997, Hoering & Ford, 1960, Minagawa &  
408 Wada, 1986). However, we note that atmospheric deposition of N has a similarly low  $\delta^{15}\text{N}$  signature  
409 (Dillon & Chanton, 2005, Hastings *et al.*, 2003, Knapp *et al.*, 2010).

410 First considering the  $\delta^{15}\text{N}$  of the source  $\text{NO}_3^-$ , we see that water column samples collected  
411 shallower than 231 m show elevation in  $\text{NO}_3^- + \text{NO}_2^- \delta^{15}\text{N}$  and  $\delta^{18}\text{O}$  as the  $\text{NO}_3^- + \text{NO}_2^-$  concentration  
412 decreases (Figs. 2 and 3). This increase in both the  $\delta^{15}\text{N}$  and  $\delta^{18}\text{O}$  of  $\text{NO}_3^- + \text{NO}_2^-$  reflects  $\text{NO}_3^-$   
413 assimilation, as is commonly observed below the euphotic zone (Granger *et al.*, 2004, Knapp *et al.*,  
414 2008, Wankel *et al.*, 2007), and thus does not represent the  $\delta^{15}\text{N}$  of the source  $\text{NO}_3^-$ . Given the  
415 difficulty in identifying the precise  $\text{NO}_3^- + \text{NO}_2^-$  source depth, we evaluate a range in  $\text{NO}_3^- + \text{NO}_2^- \delta^{15}\text{N}$   
416 end-members, including the shallow  $\text{NO}_3^- + \text{NO}_2^- \delta^{15}\text{N}$  minima in each profile, as well as the  $\text{NO}_3^- + \text{NO}_2^-$   
417  $\delta^{15}\text{N}$  in the sample collected immediately below the  $\delta^{15}\text{N}$  minima, in the  $\delta^{15}\text{N}$  budget calculations (Eqn.  
418 1) (Table I). Using a range of  $\text{NO}_3^- + \text{NO}_2^- \delta^{15}\text{N}$  values for the end-member when calculating the  
419 importance and rate of  $\text{N}_2$  fixation allows for variability in the depth from which  $\text{NO}_3^- + \text{NO}_2^-$  is being

420 mixed into the euphotic zone via, e.g., internal waves breaking near the continental shelf (Sharples *et*  
421 *al.*, 2009, Sharples *et al.*, 2007) and/or eddy pumping (Falkowski *et al.*, 1991).

422 Next, we consider the mass flux and isotopic composition of N loss pathways from the euphotic  
423 zone. The two loss terms included in the  $\delta^{15}\text{N}$  budget calculations are the  $\text{PN}_{\text{sink}}$  flux and zooplankton  
424 excretion. As described above, the  $\text{PN}_{\text{sink}}$  flux is roughly an order of magnitude larger than the  
425 zooplankton excretion flux (Tables I and II, Fig. 6). Because the  $\delta^{15}\text{N}$  of zooplankton excretion is lower  
426 than the  $\delta^{15}\text{N}$  of the  $\text{PN}_{\text{sink}}$  flux, the  $\delta^{15}\text{N}$  of the combined export fluxes is close to, but up to 0.3‰  
427 lower than, the  $\delta^{15}\text{N}$  of the  $\text{PN}_{\text{sink}}$  flux. Including the mass-weighted  $\delta^{15}\text{N}$  of the zooplankton excretion  
428 flux estimated according to Checkley and Miller (1989) (Table II) together with the  $\text{PN}_{\text{sink}}$  flux  
429 modifies the  $\delta^{15}\text{N}$  of the combined flux most significantly for C2, where it increases the importance of  
430  $\text{N}_2$  fixation from supporting ~10 to 18% of export production. When evaluating the  $\delta^{15}\text{N}$  budgets, we  
431 include both the range in the  $\delta^{15}\text{N}$  of the  $\text{NO}_3^- + \text{NO}_2^-$  end-member as well as the standard deviation  
432 associated with the  $\text{PN}_{\text{sink}}$   $\delta^{15}\text{N}$  measurement in our uncertainty estimates (Table I).

433 Using these constraints in Eqn. 2 indicates that  $\text{N}_2$  fixation was not detected as a N source  
434 supporting export production in four of the five cycles (Table I). This is qualitatively evident from  
435 comparing the  $\delta^{15}\text{N}$  of the dominant N loss term, the  $\text{PN}_{\text{sink}}$  flux, with the  $\delta^{15}\text{N}$  of subsurface  $\text{NO}_3^-$   
436  $+ \text{NO}_2^-$  (Fig. 2), and is consistent with the low abundance of *Trichodesmium* spp. in this study, <10  
437 trichomes  $\text{L}^{-1}$  (Fig. 5) (Selph *et al.*, 2021) compared with prior work where >2000 trichomes  $\text{L}^{-1}$  have  
438 been observed in the tropical North Atlantic, e.g. (Capone *et al.*, 1998, Capone *et al.*, 1997, Carpenter  
439 *et al.*, 2004). We see that the  $\delta^{15}\text{N}$  of the  $\text{PN}_{\text{sink}} +$  zooplankton excretion fluxes is nearly always higher  
440 than the  $\delta^{15}\text{N}$  of subsurface  $\text{NO}_3^- + \text{NO}_2^-$  (Fig. 2, Tables I and II). Only in C2 during the 2017 cruise was  
441 the  $\delta^{15}\text{N}$  of the combined export fluxes lower than the  $\delta^{15}\text{N}$  of subsurface  $\text{NO}_3^- + \text{NO}_2^-$  (i.e., 2.6‰ vs. 3.1  
442 to 3.7‰, respectively) (Fig. 2) (Table I), allowing for an input from a low- $\delta^{15}\text{N}$  N source to balance the  
443  $\delta^{15}\text{N}$  of N inputs to and loss from the euphotic zone.  $\text{N}_2$  fixation is estimated to have supported  $18 \pm 8\%$   
444 of export production during C2 (Table I). Multiplying this fractional importance of  $\text{N}_2$  fixation by the  
445 combined  $\text{PN}_{\text{sink}}$  and zooplankton excretion fluxes yields an estimated  $\text{N}_2$  fixation rate of  $90 \pm 40 \mu\text{mol}$   
446  $\text{N m}^{-2} \text{d}^{-1}$  during C2 (Table I). Additionally, the range in the  $\delta^{15}\text{N}$  of subsurface  $\text{NO}_3^- + \text{NO}_2^-$ , the large  
447 standard deviation associated with the  $\text{PN}_{\text{sink}}$   $\delta^{15}\text{N}$  measurement, and the high  $\text{PN}_{\text{sink}}$  flux indicates that  
448  $\text{N}_2$  fixation during C3 supported  $0 \pm 30\%$  of export production, corresponding to  $\text{N}_2$  fixation rates of  $0$   
449  $\pm 336 \mu\text{mol N m}^{-2} \text{d}^{-1}$  (Table I). The detection of  $\text{N}_2$  fixation during the 2017 and not 2018 cycles is  
450 consistent with the higher, albeit still very low, abundance of *Trichodesmium* spp. in 2017 vs. 2018  
451 (Fig. 5) (Selph *et al.*, 2021). These geochemically-derived  $\text{N}_2$  fixation rates are also consistent with the

452 range of previously reported  $^{15}\text{N}_2$  uptake rates from the northern Gulf of Mexico (Redalje *et al.*, 2019)  
453 and references therein). In particular, (Weber *et al.*, 2016) reported low rates of 0.07 to 0.37 nmol N L $^{-1}$   
454 d $^{-1}$  in July 2013 near the northern Gulf of Mexico shelf break, while (Holl *et al.*, 2007) reported July  
455 2000 rates of  $85 \pm 18 \mu\text{mol N m}^{-2} \text{ d}^{-1}$  from sites near to this study area. This range in previously  
456 reported  $^{15}\text{N}_2$  uptake rates largely brackets the geochemical estimates of N<sub>2</sub> fixation rates from this  
457 study (Table I). The N<sub>2</sub> fixation rates estimated from these  $\delta^{15}\text{N}$  budgets are relatively low compared  
458 with those found throughout the global ocean (Luo *et al.*, 2012), and are consistent with previous work  
459 that found a minor role for N<sub>2</sub> fixation supporting export production in the nearby Sargasso Sea  
460 (Altabet, 1988, Fawcett *et al.*, 2011, Knapp *et al.*, 2005).

461 We note that low rates of N<sub>2</sub> fixation ( $<50 \mu\text{mol N m}^{-2} \text{ d}^{-1}$ ) by all diazotrophs may have  
462 occurred in the study region and not been detected by the  $\delta^{15}\text{N}$  budget (Knapp *et al.*, 2005). However,  
463 prior work in the Arabian Sea comparing *Trichodesmium* spp. trichome abundance and PN<sub>sink</sub>  $\delta^{15}\text{N}$  only  
464 observed a depression in the  $\delta^{15}\text{N}$  of PN<sub>sink</sub> when  $>2000$  trichomes L $^{-1}$  were observed (Capone *et al.*,  
465 1998). To explore the quantitative potential for N<sub>2</sub> fixation by *Trichodesmium* spp. at the trichome  
466 abundances observed in this study to influence the  $\delta^{15}\text{N}$  of PN<sub>susp</sub> and/or the  $\delta^{15}\text{N}$  of DON, we consider  
467 the following. If there were 10 *Trichodesmium* spp. trichomes L $^{-1}$  in all of our study locations and times  
468 (Fig. 5) (Selph *et al.*, 2021) fixing at a rate of 1.0 pmol N trichome $^{-1}$  hr $^{-1}$  (Capone *et al.*, 1998), and N<sub>2</sub>  
469 fixation occurred over a 12-hr photoperiod, that would correspond to 120 pM N fixed d $^{-1}$ . We could  
470 further make the (unrealistic) assumption that all of that newly fixed N accumulated as DON, none  
471 went into *Trichodesmium* spp. biomass, none went into higher trophic levels, no *Trichodesmium* spp.  
472 sank out (Hewson *et al.*, 2007, Marumo & Asaoka, 1974), and none of the DON was advected away  
473 due to circulation. Making the same assumptions to maximize newly fixed N accumulation in the DON  
474 pool, and sustaining that rate of N<sub>2</sub> fixation over 100 days, this would only correspond to an  
475 accumulation of 12 nM DON. This quantity of newly fixed N would not be detectable in terms of  
476 concentration or isotopic composition in the DON or PN<sub>susp</sub> pools (Knapp *et al.*, 2008, Knapp *et al.*,  
477 2005, Knapp *et al.*, 2011). In contrast to the mass and isotopic inertia of the PN<sub>susp</sub> and especially the  
478 DON pools, the short time period over which the PN<sub>sink</sub> flux integrates over means the PN<sub>sink</sub> flux is the  
479 most responsive to small changes in the relative source of new N fueling export, and thus the best target  
480 for detecting N<sub>2</sub> fixation inputs (Altabet, 1988, Karl *et al.*, 1997). Given that Thorpe-scale analyses  
481 indicate that vertical NO<sub>3</sub> $^{-}$  transport at the time of sampling was low, N fueling the PN<sub>sink</sub> flux may have  
482 originated from upwelling of NO<sub>3</sub> $^{-}$  near the shelf break (Sharples *et al.*, 2009, Sharples *et al.*, 2007) and  
483 lateral advection of resulting organic N (Kelly *et al.*, 2021). Finally, we note that while we have

484 assumed that any low- $\delta^{15}\text{N}$  inputs to the system are from  $\text{N}_2$  fixation, the rate of  $\text{N}_2$  fixation estimated  
485 by the  $\delta^{15}\text{N}$  budget for Cycle 2, 90  $\mu\text{mol N m}^{-2} \text{d}^{-1}$  (Table I) is comparable to rates of atmospheric  $\text{NO}_3^-$   
486 +  $\text{NO}_2^-$  deposition in the region, 20 to 30  $\mu\text{mol N m}^{-2} \text{d}^{-1}$  (Hastings *et al.*, 2003, Katz *et al.*, 2009,  
487 Prospero *et al.*, 1996), which has a similarly low  $\delta^{15}\text{N}$  (Dillon & Chanton, 2005, Hastings *et al.*, 2003,  
488 Knapp *et al.*, 2010). Given the low diazotroph abundance observed on these cruises (Selph *et al.*, 2021),  
489 atmospheric deposition of low- $\delta^{15}\text{N}$  N may contribute to the low- $\delta^{15}\text{N}$   $\text{PN}_{\text{sink}}$  flux observed in Cycle 2.  
490

#### 491 **Mixed layer vs. sub-euphotic zone $\text{PN}_{\text{sink}}$ $\delta^{15}\text{N}$ : the $\delta^{15}\text{N}$ associated with regenerated production**

492 To the best of our knowledge, the  $\text{PN}_{\text{sink}}$  flux and its  $\delta^{15}\text{N}$  have not been reported from sediment  
493 traps deployed *within* the euphotic zone before. The results from this study show that the  $\text{PN}_{\text{sink}}$  flux  
494 leaving the upper euphotic zone typically exceeds the  $\text{PN}_{\text{sink}}$  flux leaving the base of the euphotic zone.  
495 On the NF1802 cruise, the  $\text{PN}_{\text{sink}}$  flux in the sub-euphotic zone trap was 81% (C4) and 82% (C5) of the  
496  $\text{PN}_{\text{sink}}$  flux captured in the 60-m trap. On the NF1704 cruise, this ratio varied from 30 to 112%  
497 (although the C3 measurement of 112% was not significantly different from the  $\text{PN}_{\text{sink}}$  flux measured in  
498 the 60-m trap) (Table I). Taken together, these results suggest that more particles were consumed in the  
499 vicinity of the deep chlorophyll maximum than were produced at that depth, with the net consumption  
500 of those particles contributing to regenerated production (Stukel *et al.*, 2021). Importantly, the  $\delta^{15}\text{N}$  of  
501 the  $\text{PN}_{\text{sink}}$  flux in the 60 m traps was 0.4 to 2.0‰ lower than that in the deeper traps in all cycles (Fig.  
502 2) (Table I). The  $\delta^{15}\text{N}$  of the  $\text{PN}_{\text{sink}}$  flux in the 50 m traps ranged from  $1.6 \pm 0.3\text{‰}$  to  $3.8 \pm 0.2\text{‰}$  (Table  
503 I). Interestingly, although perhaps not surprising given the small sample size, the  $\delta^{15}\text{N}$  increase between  
504 the 60 m and mid-depth traps does not appear related to the ratio of the  $\text{PN}_{\text{sink}}$  flux captured in the mid-  
505 depth vs. euphotic zone traps, which would be expected if flux attenuation between the traps was  
506 significant and associated with an isotope effect for N degradation. Regardless, the difference in  $\delta^{15}\text{N}$   
507 of the  $\text{PN}_{\text{sink}}$  flux between the euphotic and sub-euphotic zone is consistent with regenerated production  
508 supported by low- $\delta^{15}\text{N}$  N. This is also consistent with high rates of  $\text{NH}_4^+$  regeneration that have been  
509 found in the northern Gulf of Mexico to be the primary source of N fueling primary productivity (Bode  
510 & Dortch, 1996, Wawrik *et al.*, 2004). Regenerated  $\text{NH}_4^+$  is expected to be relatively low in  $\delta^{15}\text{N}$   
511 whether it originates from zooplankton excretion (Checkley & Miller, 1989) (Deniro & Epstein, 1981,  
512 Minagawa & Wada, 1984, Wada *et al.*, 1987), or from the degradation of DON (Knapp *et al.*, 2018a,  
513 Knapp *et al.*, 2011, Zhang *et al.*, 2020) or  $\text{PN}_{\text{susp}}$  (Hannides *et al.*, 2013). Moreover, multiple lines of  
514 evidence indicate that low- $\delta^{15}\text{N}$  forms of N accumulate in the pools associated with regenerated  
515 production. Near Bermuda, (Altabet, 1988) showed that the  $\delta^{15}\text{N}$  of  $\text{PN}_{\text{susp}}$  was ~3‰ lower than that of

516 PN<sub>sink</sub>, while the  $\delta^{15}\text{N}$  of PN<sub>sink</sub> was roughly equivalent to that of subsurface NO<sub>3</sub><sup>-</sup>. Later, (Fawcett *et al.*, 2011) found that low- $\delta^{15}\text{N}$  N sources supported the organisms carrying out regenerated production 517 near Bermuda. Additionally, they found that the  $\delta^{15}\text{N}$  of eukaryotic phytoplankton near Bermuda was 518 elevated compared to cyanobacteria and heterotrophic microbes. The  $\delta^{15}\text{N}$  of the eukaryotes was 519 similar to that of subsurface NO<sub>3</sub><sup>-</sup> and the PN<sub>sink</sub> flux, while the  $\delta^{15}\text{N}$  of cyanobacteria was similar to the 520  $\delta^{15}\text{N}$  of the bulk PN<sub>susp</sub> pool and 1 to 5‰ lower than the  $\delta^{15}\text{N}$  of subsurface NO<sub>3</sub><sup>-</sup> (Fawcett *et al.*, 2011). 521 Together, this evidence indicates that the  $\delta^{15}\text{N}$  of regenerated N retained in the euphotic zone should be 522 1 to 6‰ lower than the  $\delta^{15}\text{N}$  of the dominant source of N to surface waters, while the  $\delta^{15}\text{N}$  of fluxes of 523 N to and from should be roughly equivalent. Thus, the magnitude of the  $\delta^{15}\text{N}$  increase between the 524 shallow and mid-depth traps observed in the GoM is broadly consistent with the mechanisms outlined 525 above that would retain low- $\delta^{15}\text{N}$  material in the euphotic zone to support regenerated production and 526 permit elevated  $\delta^{15}\text{N}$  to leave via the PN<sub>sink</sub> flux.

527 Interestingly, the  $\delta^{15}\text{N}$  of the PN<sub>sink</sub> flux captured in the 60 m traps, 1.6 to 3.8‰ (Table I), is 528 relatively high compared to the  $\delta^{15}\text{N}$  of PN<sub>susp</sub>, 1.2 to 2.5‰ (Fig. 5), suggesting that the 60 m PN<sub>sink</sub> 529 flux is supported by allochthonous sources of N, such as subsurface NO<sub>3</sub><sup>-</sup>, and/or is produced by 530 organisms feeding relatively high in the food chain. Additionally, the  $\delta^{15}\text{N}$  of PN<sub>susp</sub> is elevated 531 compared to that collected near Bermuda, -1 to 0‰ (Altabet, 1988, Fawcett *et al.*, 2011). The 532 differences in the  $\delta^{15}\text{N}$  of PN<sub>susp</sub> from the GoM and near Bermuda qualitatively indicate that NO<sub>3</sub><sup>-</sup> is an 533 even more important source of new N to surface waters and/or that the ratio of new to regenerated 534 production is higher in the GoM than near Bermuda. Thus, the isotopic evidence overwhelmingly 535 indicates that subsurface NO<sub>3</sub><sup>-</sup>, and not N<sub>2</sub> fixation, supports export production in these GoM samples. 536 However, we acknowledge the possibility that PN<sub>sink</sub> with a  $\delta^{15}\text{N}$  between 2.8 to 4.9‰ could also result 537 from a linear combination of lateral sources of N with a relatively high  $\delta^{15}\text{N}$ , potentially including 538 Mississippi River and/or other coastal sources, with sources of low- $\delta^{15}\text{N}$  N, including N<sub>2</sub> fixation, 539 atmospheric deposition, and/or the consumption of DON with an isotope effect (Knapp *et al.*, 2018a, 540 Zhang *et al.*, 2020). None of our other measurements, however, show any clear evidence of substantial 541 riverine or diazotrophic influence (Selph *et al.*, 2021). We also note that our results reflect a relatively 542 short sampling period, and so does not preclude N<sub>2</sub> fixation supporting a higher fraction of export at 543 other times.

545 **CONCLUSIONS**

546 Here we use a geochemical tool, a  $\delta^{15}\text{N}$  budget, to evaluate the sources of new N fueling export  
547 production in the oceanic Gulf of Mexico. Measurements of water-column  $\text{NO}_3^- + \text{NO}_2^- \delta^{15}\text{N}$  were  
548 compared with the  $\delta^{15}\text{N}$  of  $\text{PN}_{\text{sink}}$  captured in floating sediment traps deployed below the euphotic zone.  
549 The results of the  $\delta^{15}\text{N}$  budgets indicate that subsurface  $\text{NO}_3^- + \text{NO}_2^-$ , not  $\text{N}_2$  fixation, is the dominant  
550 source of new N supporting export production in samples collected in the deep waters of the Gulf of  
551 Mexico in May of 2017 and 2018. Geochemically estimated  $\text{N}_2$  fixation rates, when  $\text{N}_2$  fixation was  
552 detected at all, were low and consistent with prior  $^{15}\text{N}_2$  uptake rates reported from the northern Gulf of  
553 Mexico (Holl *et al.*, 2007). We also report the first measurements of DON  $\delta^{15}\text{N}$  from the Gulf of  
554 Mexico, which are similar to prior observations from the Sargasso Sea (Knapp *et al.*, 2005, Knapp *et*  
555 *al.*, 2011). Finally, the difference in the  $\delta^{15}\text{N}$  of  $\text{PN}_{\text{sink}}$  collected in the shallow vs. mid-depth sediment  
556 traps is consistent with regenerated production having a low  $\delta^{15}\text{N}$  compared to the  $\delta^{15}\text{N}$  of the  $\text{PN}_{\text{sink}}$   
557 flux captured below the euphotic zone.

## 558 **ACKNOWLEDGEMENTS**

559 We gratefully acknowledge the crew and science parties on the *NOAA Ship* Nancy Foster cruises who  
560 collected these samples as well as colleagues in the BLOOFINZ-GoM project for discussions.

## 561 **FUNDING**

562 This work was supported by a National Oceanic and Atmospheric Administration's RESTORE Program  
563 Grant (Project Title: Effects of nitrogen sources and plankton food-web dynamics on habitat quality for  
564 the larvae of Atlantic bluefin tuna in the Gulf of Mexico) under federal funding opportunity NOAA-  
565 NOS-NCCOS-2017-2004875. <https://restoreactscienceprogram.noaa.gov/funded-projects/bluefin-tuna-larvae>. This study acknowledges BLOOFINZ Program support from National Oceanic and  
566 Atmospheric Administration awards NA15OAR4320071 (to MRL), NA16NMF4320058 (to KES),  
567 NA15OAR4320064 (to ANK and MRS) and U.S. National Science Foundation award OCE-1851558  
568 (MRL) and OCE-1851347 (ANK, MRS).

## 570 **DATA ARCHIVING**

571 Data presented here have been submitted to the National Oceanic and Atmospheric Administration's  
572 (NOAA) National Centers for Environmental Information (NCEI) data repository, and are also archived

573 at the BCO-DMO (Biological and Chemical Oceanography Data Management Office) site:  
574 <https://www.bco-dmo.org/project/819488>.

575  
576  
577 **REFERENCES**  
578

579 Altabet, M. A. (1988) Variations in Nitrogen Isotopic Composition between Sinking and Suspended  
580 Particles - Implications for Nitrogen Cycling and Particle Transformation in the Open Ocean.  
581 *Deep-Sea Research Part a-Oceanographic Research Papers*, **35**, 535-554.

582 Altabet, M. A., Deuser, W. G., Honjo, S. and Stienen, C. (1991) Seasonal and Depth-Related Changes  
583 in the Source of Sinking Particles in the North-Atlantic. *Nature*, **354**, 136-139.

584 Amon, R. M. W., Ochoa, J., Candela, J., Sheinbaum, J., Herguera, J. C., Herzka, S. Z., Perez-Brunius,  
585 P., Hernandez-Ayon, J. M., Camacho-Ibar, V. F. and Key, R. M. (2020) Novel insights into  
586 deep ventilation of the Gulf of Mexico and its linkage to the Labrador Sea *Ocean Sciences*  
587 *Meeting*. AGU, 2020.

588 Berman-Frank, I., Cullen, J. T., Shaked, Y., Sherrell, R. M. and Falkowski, P. G. (2001) Iron  
589 availability, cellular iron quotas, and nitrogen fixation in *Trichodesmium*. *Limnology and*  
590 *Oceanography*, **46**, 1249-1260.

591 Bidigare, R. (1983) Nitrogen excretion by marine zooplankton. In: Carpente.E.J. and D. G. Capone  
592 (eds) *Nitrogen in the Marine Environment*. 1 ed. Academic Press, New York, pp. 385-409.

593 Bode, A. and Dortch, Q. (1996) Uptake and regeneration of inorganic nitrogen in coastal waters  
594 influenced by the Mississippi River spatial and seasonal variations. *Journal of Plankton*  
595 *Research*, **18**, 2251-2268.

596 Bonnet, S., Berthelot, H., Turk-Kubo, K., Fawcett, S., Rahav, E., L'helguen, S. and Berman-Frank, I.  
597 (2016) Dynamics of N2 fixation and fate of diazotroph-derived nitrogen during the VAHINE  
598 mesocosm experiment. *Biogeosciences*, **13**, 2653-2673.

599 Bourbonnais, A., Lehmann, M. F., Wanek, J. J. and Schulz-Bull, D. E. (2009) Nitrate isotope  
600 anomalies reflect N-2 fixation in the Azores Front region (subtropical NE Atlantic). *Journal of*  
601 *Geophysical Research-Oceans*, **114**.

602 Braman, R. S. and Hendrix, S. A. (1989) Nanogram Nitrite and Nitrate Determination in Environmental  
603 and Biological-Materials by Vanadium(III) Reduction with Chemi-Luminescence Detection.  
604 *Analytical Chemistry*, **61**, 2715-2718.

605 Breitbarth, E., Oschlies, A. and Laroche, J. (2007) Physiological constraints on the global distribution  
606 of *Trichodesmium* - effect of temperature on diazotrophy. *Biogeosciences*, **4**, 53-61.

607 Bronk, D. A. and Ward, B. B. (1999) Gross and net nitrogen uptake and DON release in the euphotic  
608 zone of Monterey Bay, California. *Limnology and Oceanography*, **44**, 573-585.

609 Bronk, D. A. and Ward, B. B. (2000) Magnitude of dissolved organic nitrogen release relative to gross  
610 nitrogen uptake in marine systems. *Limnology and Oceanography*, **45**, 1879-1883.

611 Bronk, D. A. and Ward, B. B. (2005) Inorganic and organic nitrogen cycling in the Southern California  
612 Bight. *Deep-Sea Research Part I-Oceanographic Research Papers*, **52**, 2285-2300.

613 Caffin, M., Foster, R., Berthelot, H., Stenegren, M., Caputo, A., Berntzo, L. and Bonnet, S. (2018) Fate  
614 of N2 fixation in the Western Tropical South Pacific Ocean: Transfert of diazotroph-derived  
615 nitrogen to non-diazotrophic communities and export of diazotrophs. *Biogeosciences Discuss.*

616 Capone, D. G., Burns, J. A., Montoya, J. P., Subramaniam, A., Mahaffey, C., Gunderson, T., Michaels,  
617 A. F. and Carpenter, E. J. (2005) Nitrogen fixation by *Trichodesmium* spp.: An important  
618 source of new nitrogen to the tropical and subtropical North Atlantic Ocean. *Global*  
619 *Biogeochemical Cycles*, **19**.

620 Capone, D. G., Subramaniam, A., Montoya, J. P., Voss, M., Humborg, C., Johansen, A. M., Siefert, R.  
621 L. and Carpenter, E. J. (1998) An extensive bloom of the N(2)-fixing cyanobacterium  
622 *Trichodesmium erythraeum* in the central Arabian Sea. *Marine Ecology-Progress Series*, **172**,  
623 281-292.

624 Capone, D. G., Zehr, J. P., Paerl, H. W., Bergman, B. and Carpenter, E. J. (1997) *Trichodesmium*, a  
625 globally significant marine cyanobacterium. *Science*, **276**, 1221-1229.

626 Capotondi, A., Alexander, M. A., Bond, N. A., Curchitser, E. N. and Scott, J. D. (2012) Enhanced  
627 upper ocean stratification with climate change in the CMIP3 models. *Journal of Geophysical  
628 Research: Oceans*, **117**.

629 Carpenter, E. J., Harvey, H. R., Fry, B. and Capone, D. G. (1997) Biogeochemical tracers of the marine  
630 cyanobacterium *Trichodesmium*. *Deep-Sea Research Part I-Oceanographic Research Papers*,  
631 **44**, 27-38.

632 Carpenter, E. J., Subramaniam, A. and Capone, D. G. (2004) Biomass and primary productivity of the  
633 cyanobacterium *Trichodesmium* spp. in the tropical N Atlantic ocean. *Deep-Sea Research Part  
634 I-Oceanographic Research Papers*, **51**, 173-203.

635 Casciotti, K. L., Sigman, D. M., Hastings, M. G., Bohlke, J. K. and Hilkert, A. (2002) Measurement of  
636 the oxygen isotopic composition of nitrate in seawater and freshwater using the denitrifier  
637 method. *Analytical Chemistry*, **74**, 4905-4912.

638 Casciotti, K. L., Trull, T. W., Glover, D. M. and Davies, D. (2008) Constraints on nitrogen cycling at  
639 the subtropical North Pacific Station ALOHA from isotopic measurements of nitrate and  
640 particulate nitrogen. *Deep-Sea Research Part II-Topical Studies in Oceanography*, **55**, 1661-  
641 1672.

642 Checkley, D. M. and Entzeroth, L. C. (1985) Elemental and Isotopic Fractionation of Carbon and  
643 Nitrogen by Marine, Planktonic Copepods and Implications to the Marine Nitrogen-Cycle.  
644 *Journal of Plankton Research*, **7**, 553-568.

645 Checkley, D. M. and Miller, C. A. (1989) Nitrogen Isotope Fractionation by Oceanic Zooplankton.  
646 *Deep-Sea Research Part a-Oceanographic Research Papers*, **36**, 1449-1456.

647 Christian, J. R., Lewis, M. R. and Karl, D. M. (1997) Vertical fluxes of carbon, nitrogen, and  
648 phosphorus in the North Pacific Subtropical Gyre near Hawaii. *Journal of Geophysical  
649 Research-Oceans*, **102**, 15667-15677.

650 Cutter, G. A., Andersson, P., Codispoti, L., Croot, P., Francois, R., Lohan, M., Obata, H. and Van Der  
651 Loeff, M. R. (2014) Sampling and Sample-handling Protocols for GEOTRACES Cruises. pp.  
652 145.

653 Deniro, M. J. and Epstein, S. (1981) Influence of Diet on the Distribution of Nitrogen Isotopes in  
654 Animals. *Geochimica Et Cosmochimica Acta*, **45**, 341-351.

655 Dillon, K. S. and Chanton, J. P. (2005) Nutrient transformations between rainfall and stormwater runoff  
656 in an urbanized coastal environment: Sarasota Bay, Florida. *Limnology and Oceanography*, **50**,  
657 62-69.

658 Dugdale, R. C. and Goering, J. J. (1967) Uptake of New and Regenerated Forms of Nitrogen in Primary  
659 Productivity. *Limnology and Oceanography*, **12**, 196-&.

660 Emerson, S. (2014) Annual net community production and the biological carbon flux in the ocean.  
661 *Global Biogeochemical Cycles*, **28**, 2013GB004680.

662 Eppley, R. W. and Peterson, B. J. (1979) Particulate organic-matter flux and planktonic new production  
663 in the deep ocean. *Nature*, **282**, 677-680.

664 Falkowski, P. G., Zieman, D., Kolber, Z. and Bienfang, P. K. (1991) Role of Eddy Pumping in  
665 Enhancing Primary Production in the Ocean. *Nature*, **352**, 55-58.

666 Fawcett, S. E., Lomas, M., Casey, J. R., Ward, B. B. and Sigman, D. M. (2011) Assimilation of  
667 upwelled nitrate by small eukaryotes in the Sargasso Sea. *Nature Geoscience*, **4**, 717-722.

668 Fujiki, L. A., Santiago-Mandujano, F., Lethaby, P., Lukas, R. and Karl, D. (2011) Hawaii Ocean Time-  
669 series Data Report 20: 2008. pp. 395.

670 Gerard, T., Lamkin, J., Kelly, T., Knapp, A., Laiz-Carrion, R., Malca, E., Selph, K., Shiroza, A., Stukel,  
671 M., Swalethorp, R., Yingling, N. and Landry, M. (In Review) Bluefin Larvae in Oligotrophic  
672 Ocean Foodwebs, Investigations of Nutrients to Zooplankton: Overview of the BLOOFINZ-  
673 Gulf of Mexico program. *Journal of Plankton Research*.

674 Granger, J., Sigman, D. M., Needoba, J. A. and Harrison, P. J. (2004) Coupled nitrogen and oxygen  
675 isotope fractionation of nitrate during assimilation by cultures of marine phytoplankton.  
676 *Limnology and Oceanography*, **49**, 1763-1773.

677 Hannides, C. C. S., Popp, B. N., Choy, C. A. and Drazen, J. C. (2013) Midwater zooplankton and  
678 suspended particle dynamics in the North Pacific Subtropical Gyre: A stable isotope  
679 perspective. *Limnology and Oceanography*, **58**, 1931 - 1946.

680 Hannides, C. C. S., Popp, B. N., Landry, M. R. and Graham, B. S. (2009) Quantification of  
681 zooplankton trophic position in the North Pacific Subtropical Gyre using stable nitrogen  
682 isotopes. *Limnology and Oceanography*, **54**, 50-61.

683 Hastings, M. G., Sigman, D. M. and Lipschultz, F. (2003) Isotopic evidence for source changes of  
684 nitrate in rain at Bermuda. *Journal of Geophysical Research-Atmospheres*, **108**.

685 Hernandez-Guerra, A. and Joyce, T. M. (2000) Water masses and circulation in the surface layers of the  
686 Caribbean at 66 W. *Geophysical Research Letters*, **27**, 3497-3500.

687 Hewson, I., Moisander, P. H., Achilles, K. M., Carlson, C. A., Jenkins, B. D., Mondragon, E. A.,  
688 Morrison, A. E. and Zehr, J. P. (2007) Characteristics of diazotrophs in surface to abyssopelagic  
689 waters of the Sargasso Sea. *Aquatic Microbial Ecology*, **46**, 15-30.

690 Hoering, T. C. and Ford, H. T. (1960) The Isotope Effect in the Fixation of Nitrogen by Azotobacter.  
691 *Journal of the American Chemical Society*, **82**, 376-378.

692 Hofmann, E. E. and Worley, S. J. (1986) An investigation of the circulation of the Gulf of Mexico.  
693 *Journal of Geophysical Research: Oceans*, **91**, 14221-14236.

694 Holl, C. M., Villareal, T. A., Payne, C. D., Clayton, T. D., Hart, C. and Montoya, J. P. (2007)  
695 Trichodesmium in the western Gulf of Mexico: 15N2-fixation and natural abundance stable  
696 isotope evidence. *Limnology and Oceanography*, **52**, 2249-2259.

697 Holmes, R. M., Aminot, A., Kerouel, R., Hooker, B. A. and Peterson, B. J. (1999) A simple and precise  
698 method for measuring ammonium in marine and freshwater ecosystems. *Canadian Journal of  
699 Fisheries and Aquatic Sciences*, **56**, 1801-1808.

700 Howe, S., Miranda, C., Hayes, C., Letscher, R. and Knapp, A. N. (2020) The dual isotopic composition  
701 of nitrate in the Gulf of Mexico and Florida Straits. *Journal of Geophysical Research: Oceans*,  
702 **125**, e2020JC016047.

703 Karl, D., Letelier, R., Tupas, L., Dore, J., Christian, J. and Hebel, D. (1997) The role of nitrogen  
704 fixation in biogeochemical cycling in the subtropical North Pacific Ocean. *Nature*, **388**, 533-  
705 538.

706 Katz, B. G., Sepulveda, A. A. and Verdi, R. J. (2009) Estimating Nitrogen Loading to Ground Water  
707 and Assessing Vulnerability to Nitrate Contamination in a Large Karstic Springs Basin, Florida.  
708 *Journal of the American Water Resources Association*, **45**, 607-627.

709 Kelly, T. B., Knapp, A. N., Landry, M. R., Selph, K. E., Shropshire, T. A., Thomas, R. and Stukel, M.  
710 R. (2021) Lateral advection supports nitrogen export in the oligotrophic open-ocean Gulf of  
711 Mexico. *Nature Communications*, **12**.

712 Knapp, A. N., Casciotti, K. L., Berelson, W. M., Prokopenko, M. G. and Capone, D. G. (2016a) Low  
713 rates of nitrogen fixation in eastern tropical South Pacific surface waters. *Proceedings of the  
714 National Academy of Sciences of the United States of America*, **113**, 4398-4403.

715 Knapp, A. N., Casciotti, K. L. and Prokopenko, M. G. (2018a) Dissolved organic nitrogen production  
716 and consumption in eastern tropical South Pacific surface waters. *Global Biogeochemical*  
717 *Cycles*, **32**.

718 Knapp, A. N., Difiore, P. J., Deutsch, C., Sigman, D. M. and Lipschultz, F. (2008) Nitrate isotopic  
719 composition between Bermuda and Puerto Rico: Implications for N(2) fixation in the Atlantic  
720 Ocean. *Global Biogeochemical Cycles*, **22**.

721 Knapp, A. N., Fawcett, S. E., Martínez-Garcia, A., Leblond, N., Moutin, T. and Bonnet, S. (2016b)  
722 Nitrogen isotopic evidence for a shift from nitrate- to diazotroph-fueled export production in the  
723 VAHINE mesocosm experiments. *Biogeosciences*, **13**, 4645-4657.

724 Knapp, A. N., Hastings, M. G., Sigman, D. M., Lipschultz, F. and Galloway, J. N. (2010) The flux and  
725 isotopic composition of reduced and total nitrogen in Bermuda rain. *Marine Chemistry*, **120**, 83-  
726 89.

727 Knapp, A. N., Mccabe, K. M., Gross, O., Leblond, N., Moutin, T. and Bonnet, S. (2018b) Distribution  
728 and rates of nitrogen fixation in the western tropical South Pacific Ocean constrained by  
729 nitrogen isotope budgets. *Biogeosciences*, **15**, 2619-2628.

730 Knapp, A. N., Sigman, D. M. and Lipschultz, F. (2005) N isotopic composition of dissolved organic  
731 nitrogen and nitrate at the Bermuda Atlantic time-series study site. *Global Biogeochemical*  
732 *Cycles*, **19**.

733 Knapp, A. N., Sigman, D. M., Lipschultz, F., Kustka, A. B. and Capone, D. G. (2011) Interbasin  
734 isotopic correspondence between upper-ocean bulk DON and subsurface nitrate and its  
735 implications for marine nitrogen cycling. *Global Biogeochemical Cycles*, **25**.

736 Koroleff, F. (1983) Determination of nutrients. In: K. Grasshoff, M. Ehrherd and K. Kremling (eds)  
737 *Methods of Seawater Analysis*. 2nd ed., pp. 125-135.

738 Kustka, A. B., Sanudo-Wilhelmy, S. A., Carpenter, E. J., Capone, D., Burns, J. and Sunda, W. G.  
739 (2003) Iron requirements for dinitrogen- and ammonium-supported growth in cultures of  
740 *Trichodesmium* (IMS 101): Comparison with nitrogen fixation rates and iron: carbon ratios of  
741 field populations. *Limnology and Oceanography*, **48**, 1869-1884.

742 Landry, M. R. and Swalethorp, R. (2021) Mesozooplankton biomass, grazing and trophic structure in  
743 the bluefin tuna spawning area of the oceanic Gulf of Mexico. *Journal of Plankton Research*,  
744 doi: 10.1093/plankt/fbab008.

745 Leichter, J. J., Paytan, A., Wankel, S. and Hanson, K. (2007) Nitrogen and oxygen isotopic signatures  
746 of subsurface nitrate seaward of the Florida Keys reef tract. *Limnology and Oceanography*, **52**,  
747 1258-1267.

748 Luo, Y.-W., Shi, D., Kranz, S. A., Hopkinson, B. M., Hong, H., Shen, R. and Zhang, F. (2019)  
749 Reduced nitrogenase efficiency dominates response of the globally important nitrogen fixer  
750 *Trichodesmium* to ocean acidification. *Nature Communications*, **10**, 1521.

751 Luo, Y. W., Doney, S. C., Anderson, L. A., Benavides, M., Berman-Frank, I., Bode, A., Bonnet, S.,  
752 Boström, K. H., Böttjer, D., Capone, D. G., Carpenter, E. J., Chen, Y. L., Church, M. J., Dore, J.  
753 E., Falcón, L. I., Fernández, A., Foster, R. A., Furuya, K., Gómez, F., Gundersen, K., Hynes, A.  
754 M., Karl, D. M., Kitajima, S., Langlois, R. J., Laroche, J., Letelier, R. M., Marañón, E.,  
755 Mcgillicuddy Jr, D. J., Moisander, P. H., Moore, C. M., Mouriño-Carballido, B., Mulholland,  
756 M. R., Needoba, J. A., Orcutt, K. M., Poulton, A. J., Rahav, E., Raimbault, P., Rees, A. P.,  
757 Riemann, L., Shiozaki, T., Subramaniam, A., Tyrrell, T., Turk-Kubo, K. A., Varela, M.,  
758 Villareal, T. A., Webb, E. A., White, A. E., Wu, J. and Zehr, J. P. (2012) Database of  
759 diazotrophs in global ocean: abundance, biomass and nitrogen fixation rates. *Earth Syst Sci  
760 Data*, **4**, 47-73.

761 Mahaffey, C., Michaels, A. F. and Capone, D. G. (2005) The conundrum of marine N(2) fixation.  
762 *American Journal of Science*, **305**, 546-595.

763 Mahowald, N. M., Engelstaedter, S., Luo, C., Sealy, A., Artaxo, P., Benitez-Nelson, C., Bonnet, S.,  
764 Chen, Y., Chuang, P. Y., Cohen, D. D., Dulac, F., Herut, B., Johansen, A. M., Kubilay, N.,  
765 Losno, R., Maenhaut, W., Paytan, A., Prospero, J. A., Shank, L. M. and Siefert, R. L. (2009)  
766 Atmospheric Iron Deposition: Global Distribution, Variability, and Human Perturbations *Annual*  
767 *Review of Marine Science*. Vol. 1. pp. 245-278.

768 Marconi, D., Sigman, D. M., Casciotti, K. L., Campbell, E. C., Weigand, M. A., Fawcett, S. E., Knapp,  
769 A. N., Rafter, P. A., Ward, B. B. and Haug, G. H. (2017) Tropical Dominance of N2 Fixation in  
770 the North Atlantic Ocean. *Global Biogeochemical Cycles*, **31**.

771 Marconi, D., Weigand, M. A., Rafter, P. A., Mcilvin, M. R., Forbes, M., Casciotti, K. L. and Sigman,  
772 D. M. (2015) Nitrate isotope distributions on the US GEOTRACES North Atlantic cross-basin  
773 section: Signals of polar nitrate sources and low latitude nitrogen cycling. *Marine Chemistry*,  
774 **177**, 143-156.

775 Marconi, D., Weigand, M. A. and Sigman, D. M. (2019) Nitrate isotopic gradients in the North Atlantic  
776 Ocean and the nitrogen isotopic composition of sinking organic matter. *Deep Sea Research Part*  
777 *I: Oceanographic Research Papers*, **145**, 109-124.

778 Marumo, R. and Asaoka, O. (1974) Distribution of pelagic blue-green algae in the North Pacific Ocean.  
779 *Journal of the Oceanographical Society of Japan*, **30**, 77-85.

780 McClelland, J. W., Holl, C. M. and Montoya, J. P. (2003) Relating low delta N-15 values of  
781 zooplankton to N-2-fixation in the tropical North Atlantic: insights provided by stable isotope  
782 ratios of amino acids. *Deep-Sea Research Part I-Oceanographic Research Papers*, **50**, 849-861.

783 Mcilvin, M. R. and Casciotti, K. L. (2011) Technical Updates to the Bacterial Method for Nitrate  
784 Isotopic Analyses. *Analytical Chemistry*, **83**, 1850-1856.

785 Minagawa, M. and Wada, E. (1984) Stepwise Enrichment of N-15 Along Food-Chains - Further  
786 Evidence and the Relation between Delta-N-15 and Animal Age. *Geochimica Et Cosmochimica  
787 Acta*, **48**, 1135-1140.

788 Minagawa, M. and Wada, E. (1986) Nitrogen Isotope Ratios of Red Tide Organisms in the East-China-  
789 Sea - a Characterization of Biological Nitrogen-Fixation. *Marine Chemistry*, **19**, 245-259.

790 Monterey, G. and Levitus, S. (1997) Seasonal Variability of Mixed Layer Depth for the World Ocean.  
791 In: D. O. C. Noaa, USA (ed) Vol. 14. NOAA, Silver Spring, MD, pp. 100.

792 Montoya, J. P., Carpenter, E. J. and Capone, D. G. (2002) Nitrogen fixation and nitrogen isotope  
793 abundances in zooplankton of the oligotrophic North Atlantic. *Limnology and Oceanography*,  
794 **47**, 1617-1628.

795 Morey, S. L., Martin, P. J., O'brien, J. J., Wallcraft, A. A. and Zavala-Hidalgo, J. (2003) Export  
796 pathways for river discharged fresh water in the northern Gulf of Mexico. *Journal of  
797 Geophysical Research: Oceans*, **108**.

798 Morrison, J. M., Merrell Jr, W. J., Key, R. M. and Key, T. C. (1983) Property distributions and deep  
799 chemical measurements within the western Gulf of Mexico. *Journal of Geophysical Research:  
800 Oceans*, **88**, 2601-2608.

801 Mulholland, M. R., Bernhardt, P. W., Heil, C. A., Bronk, D. A. and O'neil, J. M. (2006) Nitrogen  
802 fixation and release of fixed nitrogen by *Trichodesmium* spp. in the Gulf of Mexico. *Limnology  
803 and Oceanography*, **51**, 1762-1776.

804 Mulholland, M. R., Bernhardt, P. W., Ozmon, I., Procise, L. A., Garrett, B., M., O'neil, J. M., Heil, C.  
805 A. and Bronk, D. A. (2014) Contribution of diazotrophy to nitrogen inputs supporting *Karenia*  
806 *brevis* blooms in the Gulf of Mexico. *Harmful Algae*, **38**, 20-29.

807 Press, W. H., Teukolsky, S. A., Vetterling, W. T. and Flannery, B. P. (1992) *Numerical Recipes in C:  
808 The art of scientific computing*, 2nd edition. Vol., Cambridge University Press.

809 Prospero, J. M. (1996) Saharan dust transport over the North Atlantic Ocean and Mediterranean: An  
810 overview *Impact of Desert Dust across the Mediterranean*. Vol. 11. pp. 133-151.

811 Prospero, J. M., Barrett, K., Church, T., Dentener, F., Duce, R. A., Galloway, J. N., Levy, H., Moody,  
812 J. and Quinn, P. (1996) Atmospheric deposition of nutrients to the North Atlantic Basin.  
813 *Biogeochemistry*, **35**, 27-73.

814 Redalje, D. G., Ammerman, J., Herrera, J., Knapp, A., Krause, J., Valdes, D. and Hayward, A. (2019)  
815 Nutrients in the Gulf of Mexico: Distributions, Cycles, Sources, Sinks and Processes. In: T. S.  
816 Bianchi (ed) *Gulf of Mexico Origin, Waters, and Biota*. Texas A&M University Press, pp. 294.

817 Sanial, V., Moore, W. S. and Shiller, A. M. (2021) Does a bottom-up mechanism promote hypoxia in  
818 the Mississippi Bight? *Marine Chemistry*, **235**, 104007.

819 Selph, K. E., Swalethorp, R., Stukel, M. R., Kelly, T. B., Knapp, A. N., Fleming, K., Hernandez, T. and  
820 Landry, M. R. (2021) Phytoplankton community composition and biomass in the oligotrophic  
821 Gulf of Mexico. *Journal of Plankton Research*, doi: 10.1093/plankt/fbab006.

822 Sharples, J., Moore, C. M., Hickman, A. E., Holligan, P. M., Tweddle, J. F., Palmer, M. R. and  
823 Simpson, J. H. (2009) Internal tidal mixing as a control on continental margin ecosystems.  
824 *Geophysical Research Letters*, **36**.

825 Sharples, J., Tweddle, J. F., Mattias Green, J. A., Palmer, M. R., Kim, Y.-N., Hickman, A. E., Holligan,  
826 P. M., Moore, C. M., Rippeth, T. P., Simpson, J. H. and Krivtsov, V. (2007) Spring-neap  
827 modulation of internal tide mixing and vertical nitrate fluxes at a shelf edge in summer.  
828 *Limnology and Oceanography*, **52**, 1735-1747.

829 Shi, D., Kranz, S. A., Kim, J.-M. and Morel, F. M. M. (2012) Ocean acidification slows nitrogen  
830 fixation and growth in the dominant diazotroph *Trichodesmium* under low-iron conditions.  
831 *Proceedings of the National Academy of Sciences of the United States of America*, **109**, E3094-  
832 100.

833 Shiozaki, T., Bombar, D., Riemann, L., Sato, M., Hashihama, F., Kodama, T., Tanita, I., Takeda, S.,  
834 Saito, H., Hamasaki, K. and Furuya, K. (2018) Linkage Between Dinitrogen Fixation and  
835 Primary Production in the Oligotrophic South Pacific Ocean. *Global Biogeochemical Cycles*,  
836 **32**, 1028-1044.

837 Sigman, D. M., Casciotti, K. L., Andreani, M., Barford, C., Galanter, M. and Bohlke, J. K. (2001) A  
838 bacterial method for the nitrogen isotopic analysis of nitrate in seawater and freshwater.  
839 *Analytical Chemistry*, **73**, 4145-4153.

840 Sohm, J. A., Webb, E. A. and Capone, D. G. (2011) Emerging patterns of marine nitrogen fixation.  
841 *Nature Reviews Microbiology*, **9**, 499-508.

842 Stal, L. J. (2009) Is the distribution of nitrogen-fixing cyanobacteria in the oceans related to  
843 temperature? *Environmental Microbiology*, **11**, 1632-1645.

844 Stenegren, M., Caputo, A., Berg, C., Bonnet, S. and Foster, R. A. (2018) Distribution and drivers of  
845 symbiotic and free-living diazotrophic cyanobacteria in the western tropical South Pacific.  
846 *Biogeosciences*, **15**, 1559-1578.

847 Stukel, M. R., Décima, M., Landry, M. R. and Selph, K. E. (2018) Nitrogen and Isotope Flows Through  
848 the Costa Rica Dome Upwelling Ecosystem: The Crucial Mesozooplankton Role in Export  
849 Flux. *Global Biogeochemical Cycles*, **32**, 1815-1832.

850 Stukel, M. R., Kelly, T. B., Landry, M. R., Selph, K. E. and Swalethorp, R. (2021) Sinking carbon,  
851 nitrogen, and pigment flux within and beneath the euphotic zone in the oligotrophic, open-ocean  
852 Gulf of Mexico. *Journal of Plankton Research*, doi: 10.1093/plankt/fbab001.

853 Wada, E., Terazaki, M., Kabaya, Y. and Nemoto, T. (1987) N-15 and C-13 Abundances in the  
854 Antarctic Ocean with Emphasis on the Biogeochemical Structure of the Food Web. *Deep-Sea*  
855 *Research Part a-Oceanographic Research Papers*, **34**, 829-841.

856 Wankel, S. D., Kendall, C., Pennington, J. T., Chavez, F. P. and Paytan, A. (2007) Nitrification in the  
857 euphotic zone as evidenced by nitrate dual isotopic composition: Observations from Monterey  
858 Bay, California. *Global Biogeochemical Cycles*, **21**.

859 Ward, B. B. and Bronk, D. A. (2001) Net nitrogen uptake and DON release in surface waters:  
 860 importance of trophic interactions implied from size fractionation experiments. *Marine  
 861 Ecology-Progress Series*, **219**, 11-24.

862 Wawrik, B., Paul, J. H., Bronk, D. A., John, D. and Gray, M. (2004) High rates of ammonium recycling  
 863 drive phytoplankton productivity in the offshore Mississippi River plume. *Aquatic Microbial  
 864 Ecology*, **35**, 175-184.

865 Weber, S. C., Peterson, L., Battles, J. J., Roberts, B. J., Peterson, R. N., Hollander, D. J., Chanton, J. P.,  
 866 Joye, S. B. and Montoya, J. P. (2016) Hercules 265 rapid response: Immediate ecosystem  
 867 impacts of a natural gas blowout incident. *Deep-Sea Research Part II*, **129**, 66-76.

868 Weigand, M. A., Foriel, J., Barnett, B., Oleynik, S. and Sigman, D. M. (2016) Updates to  
 869 instrumentation and protocols for isotopic analysis of nitrate by the denitrifier method. *Rapid  
 870 Communications in Mass Spectrometry*, **30**, 1365-1383.

871 Westberry, T. K., Williams, P. J. L. B. and Behrenfeld, M. J. (2012) Global net community production  
 872 and the putative net heterotrophy of the oligotrophic oceans. *Global Biogeochemical Cycles*, **26**.

873 White, A. E., Foster, R. A., Benitez-Nelson, C. R., Masqué, P., Verdeny, E., Popp, B. N., Arthur, K. E.  
 874 and Prahl, F. G. (2013) Nitrogen fixation in the Gulf of California and the Eastern Tropical  
 875 North Pacific. *Progress in Oceanography*, **109**, 1-17.

876 White, A. E., Granger, J., Selden, C., Gradoville, M. R., Potts, L., Bourbonnais, A., Fulweiler, R. W.,  
 877 Knapp, A. N., Mohr, W., Moisander, P. H., Tobias, C. R., Caffin, M., Wilson, S. T., Benavides,  
 878 M., Bonnet, S., Mulholland, M. R. and Chang, B. X. (2020) A critical review of the  $^{15}\text{N}_2$  tracer  
 879 method to measure diazotrophic production in pelagic ecosystems. *Limnology and  
 880 Oceanography: Methods*, **18**, 129-147.

881 Wilson, W. D. and Johns, W. E. (1997) Velocity structure and transport in the Windward Islands  
 882 Passages. *Deep Sea Research Part I: Oceanographic Research Papers*, **44**, 487-520.

883 Yingling, N., Kelly, T. B., Shropshire, T. A., Landry, M. R., Selph, K. E., Knapp, A. N., Kranz, S. A.  
 884 and Stukel, M. R. (2021) Taxon-specific phytoplankton growth, nutrient utilization, and light  
 885 limitation in the oligotrophic Gulf of Mexico. *Journal of Plankton Research*.

886 Zhang, R., Wang, X. T., Ren, H., Huang, J., Chen, M. and Sigman, D. M. (2020) Dissolved Organic  
 887 Nitrogen Cycling in the South China Sea From an Isotopic Perspective. *Global Biogeochemical  
 888 Cycles*, **34**, e2020GB006551.

889 **Legends for Tables and Figures**

890 Table I. The mass and isotopic composition of the sinking particulate nitrogen flux captured in drifting  
 891 sediment traps, and results of  $\delta^{15}\text{N}$  budgets for traps deployed below the base of the euphotic zone for  
 892 2017 and 2018 cruises, including the range in  $\text{NO}_3^- + \text{NO}_2^-$   $\delta^{15}\text{N}$  end-member, fraction of export  
 893 supported by  $\text{N}_2$  fixation ("F<sub>N2fix</sub>") and  $\text{N}_2$  fixation rate determined by multiplying PN<sub>sink</sub> flux by F<sub>N2fix</sub>.  
 894 The fractional importance of  $\text{N}_2$  fixation and geochemical  $\text{N}_2$  fixation rate estimates include  
 895 contributions from zooplankton excretion at depth (Table II), see text for details.

896 Table II. The ammonia+urea excretion flux by vertically migrating zooplankton and its estimated  
 897 isotopic composition. All zooplankton size fractions were summed and the bulk zooplankton isotopic  
 898 composition represents the mass-weighted mean  $\delta^{15}\text{N}$  of all zooplankton size fractions in each cycle.  
 899 The estimated  $\delta^{15}\text{N}$  of the excretion flux is calculated by: 1) assuming a difference of 3‰ between the  
 900  $\delta^{15}\text{N}$  of bulk zooplankton biomass and the  $\delta^{15}\text{N}$  of the excretion (next to last column) (Checkley and  
 901 Miller, 1989), and, 2) modeling zooplankton size and fraction of biomass below the euphotic zone, and  
 902 assuming an isotope effect of 5‰ for zooplankton excretion (last column) (Stukel *et al.*, 2018). See text  
 903 for details.

907 Table III. The mean concentration and  $\delta^{15}\text{N}$  of suspended particulate organic nitrogen (PN<sub>susp</sub>)  $\pm$  1  
908 standard deviation with depth for each Cycle.

909 Figure 1. Map of sampling locations for the 2017 (C1, pink, C2, light blue, and C3, green) and 2018  
910 (C4, red, and C5, dark blue) cruises.

911 Figure 2. Measurements supporting  $\delta^{15}\text{N}$  budget calculations, including the concentration (open circles)  
912 and  $\delta^{15}\text{N}$  (filled circles) of  $\text{NO}_3^- + \text{NO}_2^-$  as well as PN<sub>sink</sub>  $\delta^{15}\text{N}$  (filled triangles) from the 2017 (a) and  
913 2018 (b) cruises, with “C1” represented by solid pink lines, “C2” represented by dashed light blue lines,  
914 “C3” represented by dotted green lines, “C4” represented by solid red lines, and “C5” represented by  
915 dashed dark blue lines. The arrows on the x-axes represent the  $\delta^{15}\text{N}$  associated with  $\text{N}_2$  fixation inputs.  
916 Error bars represent  $\pm 1$  S.D. and are smaller than the symbol size for  $\text{NO}_3^- + \text{NO}_2^-$  concentration and  
917 often the  $\text{NO}_3^- + \text{NO}_2^- \delta^{15}\text{N}$  measurements.

918  
919 Figure 3. The concentration,  $\delta^{15}\text{N}$ , and  $\delta^{18}\text{O}$  of  $\text{NO}_3^- + \text{NO}_2^-$  from the NF1704 (filled squares) and  
920 NF1802 (filled circles) cruises plotted vs. depth (a, b, and c, respectively) and on sigma theta surfaces  
921 (d, e, and f, respectively). Error bars represent  $\pm 1$  S.D. and are smaller than the symbol size for  $\text{NO}_3^- + \text{NO}_2^-$   
922 concentration. Colors follow from Figure 2.

923  
924 Figure 4. Location of sampling during the 2018 cruise (a) with concentration (b) and  $\delta^{15}\text{N}$  (c) of DON  
925 in the upper 150 m. Cross section begins at southwest end and finishes at northeast end of transect.  
926 Salinity contours overlay DON concentration and  $\delta^{15}\text{N}$  color contours in panels (b) and (c),  
927 respectively.

928  
929 Figure 5. Cycle-mean ( $\pm 1$  S.D., with cycle colors following from previous figures) upper water column  
930 *Trichodesmium* spp. trichome abundance (bow tie symbol) (a); chlorophyll *a* concentration (filled  
931 diamonds) (b), PN<sub>susp</sub> concentration (open circles) and DON concentration (filled circles) (c), and  
932 PN<sub>susp</sub>  $\delta^{15}\text{N}$  (open circles) and DON  $\delta^{15}\text{N}$  (filled circles) (d).

933  
934 Figure 6. Schematic of nitrogen pools and fluxes to, from, and within the euphotic zone in the  
935 oligotrophic Gulf of Mexico. Dashed lines represent low- $\delta^{15}\text{N}$  fluxes, with solid lines representing  
936 transfers of relatively high  $\delta^{15}\text{N}$ . The mean flux magnitudes for fluxes out of the euphotic zone  
937 quantified in this study, PN<sub>sink</sub> and zooplankton excretion, are shown in bold, with units of  $\mu\text{mol N m}^{-2}$   
938  $\text{d}^{-1}$ , as well as their representative isotopic composition. The mean concentrations and  $\delta^{15}\text{N}$  of PN<sub>susp</sub>  
939 and DON in the euphotic are reported with concentration in units of  $\mu\text{M}$ . The  $\delta^{15}\text{N}$  budgets described in  
940 the text compare the  $\delta^{15}\text{N}$  of subsurface  $\text{NO}_3^-$  with the  $\delta^{15}\text{N}$  of the PN<sub>sink</sub> flux and the estimate of  
941 zooplankton excretion below the euphotic zone. Regenerated  $\text{NH}_4^+$  represents an important low- $\delta^{15}\text{N}$  N  
942 source fueling phytoplankton in the euphotic zone.

943  
944  
945  
946  
947  
948

Table I. Mass and isotopic composition of sinking particulate nitrogen flux captured in floating sediment traps and fraction of export supported by  $N_2$  fixation, as well as geochemically-based  $N_2$  fixation rate. Fractional importance of  $N_2$  fixation and geochemical  $N_2$  fixation rate estimates include contributions from zooplankton excretion at depth (Table II), see text for details.

Year	Cycle	Trap Depth (m)	Mass flux range (mmol N m <sup>-2</sup> d <sup>-1</sup> )	Mean mass flux ( $\pm 1$ S.D.) (mmol N m <sup>-2</sup> d <sup>-1</sup> )	PN <sub>sink</sub> δ <sup>15</sup> N range (% vs. $N_2$ in air)	Mean PN <sub>sink</sub> δ <sup>15</sup> N ( $\pm 1$ S.D.) (% vs. $N_2$ in air)	NO <sub>3</sub> <sup>-</sup> +NO <sub>2</sub> <sup>-</sup> δ <sup>15</sup> N (% vs. $N_2$ in air)	F <sub>N2fix</sub> (%)	N <sub>2</sub> fix rate ( $\mu\text{mol N m}^{-2} \text{d}^{-1}$ )
2017	1	60	1.01 - 2.10	1.53 ± 0.6	2.7 - 3.2	2.9 ± 0.3	3.2 to 3.8‰	0	0
		140	0.44 - 0.49	0.46 ± 0.02	4.5 - 5.1	4.9 ± 0.3			
		231	0.17 - 0.20	0.19 ± 0.02	4.1 - 4.5	4.2 ± 0.3			
2017	2	60	0.79 - 0.88	0.82 ± 0.05	1.9 - 2.9	2.5 ± 0.6	3.1 to 3.7‰	18 ± 8	90 ± 40
		140	0.38 - 0.72	0.52 ± 0.18	2.8 - 2.9	2.9 ± 0.1			
		231	0.19 - 0.25	0.22 ± 0.03	3.3 - 3.9	3.6 ± 0.3			
2017	3	60	0.83 - 1.28	0.98 ± 0.26	1.4 - 1.8	1.6 ± 0.3	2.8 to 3.8‰	0 ± 30	0 ± 336
		140	1.01 - 1.34	1.1 ± 0.18	1.0 - 1.3	3.9 ± 1.5			
		231	0.32 - 0.55	0.4 ± 0.13	3.5 - 3.9	3.6 ± 0.2			
2018	4	60	0.45 - 0.62	0.59 ± 0.04	2.4 - 2.7	2.5 ± 0.2	2.0 to 2.2‰	0	0
		151	0.38 - 0.57	0.47 ± 0.10	3.4 - 3.7	3.8 ± 0.4			
		231	0.23 - 0.25	0.25 ± 0.01	4.5 - 4.9	4.7 ± 0.2			
2018	5	60	1.00 - 1.13	1.08 ± 0.07	3.6 - 4.0	3.8 ± 0.2	2.9 to 3.8‰	0	0
		117	0.67 - 1.03	0.87 ± 0.18	4.5 - 4.7	4.6 ± 0.1			
		231	0.30 - 0.34	0.32 ± 0.02	4.8 - 5.1	5.0 ± 0.2			

Table II. Ammonia excretion flux by diel vertically migrating zooplankton and estimated isotopic composition. The same number of net tows (n) per cycle were used to determine the zooplankton excretion flux as well as the mean δ<sup>15</sup>N of zooplankton. Within each tow, zooplankton were sorted into five size classes. The ZP δ<sup>15</sup>N reported below represents the mass-weighted mean of all size classes from all tows per cycle. See Landry and Swalethorpe (2021) for additional details.

Year	Cycle	Export Depth (m)	Net tows (n)	Mass flux range (μmol N m <sup>-2</sup> d <sup>-1</sup> )	Mean mass Flux ( $\pm 1$ S.D.) (μmol N m <sup>-2</sup> d <sup>-1</sup> )	Mean ZP δ <sup>15</sup> N ( $\pm 1$ S.D.) (% vs. $N_2$ in air)	Excreted δ <sup>15</sup> N* ( $\pm 1$ S.D.) (% vs. $N_2$ in air)	Excreted δ <sup>15</sup> N# ( $\pm$ error) (% vs. $N_2$ in air)
2017	1	100	7	-37.0 to 49.2	19.6 ± 49.5	6.0 ± 1.3	3.0 ± 1.3	1.7 ± 0.7
		100	4	49.0 to 119.8	84.4 ± 50.1	4.1 ± 1.2	1.1 ± 1.2	-1.8 ± 0.4
		100	8	-52.0 to 126.8	41.9 ± 85.5	4.1 ± 1.2	1.1 ± 1.2	-1.1 ± 0.4
2018	4	100	9	-69.5 to 138.5	37.7 ± 87.2	3.6 ± 1.4	0.6 ± 1.4	-1.1 ± 0.2
		100	9	81.9 to 309.0	171.7 ± 103.3	6.1 ± 1.0	3.1 ± 1.0	0.2 ± 0.3

\*Estimated according to Checkley and Miller (1989), where δ<sup>15</sup>N of excretion flux is 3‰ lower than the δ<sup>15</sup>N of zooplankton

#Estimated using a 5% isotopic effect for zooplankton excretion as outlined in Stukel et al. (2018).

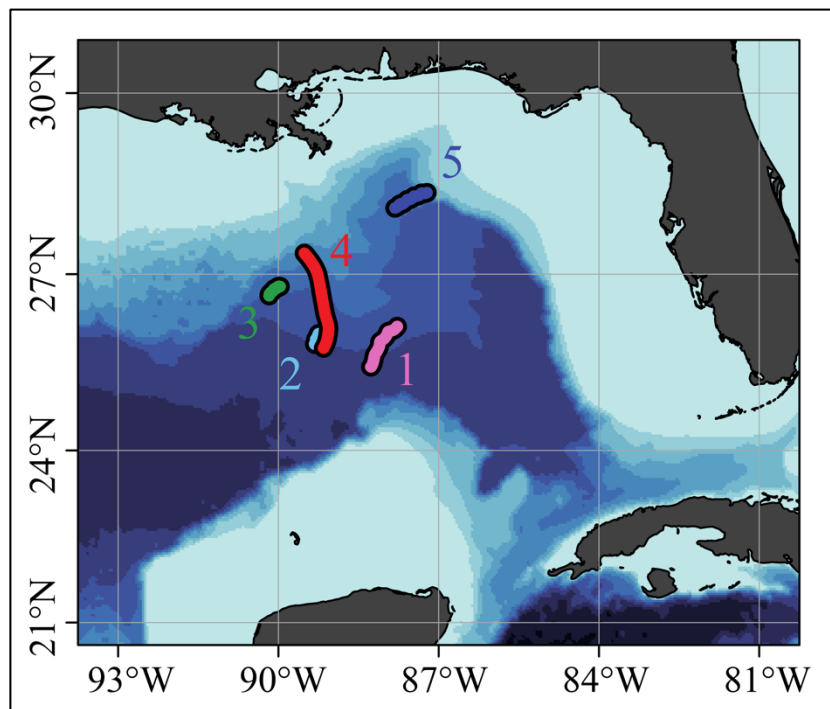
949  
950  
951  
952

Table III. Mean concentration and nitrogen isotopic composition of suspended particulate organic nitrogen (PN<sub>susp</sub>)  $\pm$  1 standard deviation.

Cycle	Depth	PN <sub>susp</sub> ( $\mu$ M) ( $\pm$ 1 S.D.)	PN <sub>susp</sub> $\delta^{15}\text{N}$ ( $\pm$ 1 S.D.)	n
1	5	1.25 $\pm$ 0.23	1.41 $\pm$ 0.75	4
1	20	0.95 $\pm$ 0.05	1.47 $\pm$ 0.87	4
1	30	0.89 $\pm$ 0.11	1.43 $\pm$ 0.72	4
1	50	1.10 $\pm$ 0.24	1.92 $\pm$ 0.50	4
1	70	0.93 $\pm$ 0.21	2.22 $\pm$ 1.44	4
1	100	1.02 $\pm$ 0.08	1.26 $\pm$ 0.91	4
2	5	1.13 $\pm$ 0.35	1.05 $\pm$ 1.37	3
2	20	0.90 $\pm$ 0.25	1.01 $\pm$ 1.18	3
2	40	0.88 $\pm$ 0.15	1.54 $\pm$ 0.97	3
2	60	0.90 $\pm$ 0.14	1.22 $\pm$ 0.75	3
2	80	1.09 $\pm$ 0.25	1.57 $\pm$ 1.59	3
2	115	0.85 $\pm$ 0.05	1.92 $\pm$ 1.26	3
3	5	1.26 $\pm$ 0.26	1.03 $\pm$ 0.49	4
3	20	1.10 $\pm$ 0.22	0.94 $\pm$ 1.27	4
3	40	1.21 $\pm$ 0.53	1.37 $\pm$ 0.31	4
3	60	1.17 $\pm$ 0.14	2.33 $\pm$ 0.75	4
3	80	1.02 $\pm$ 0.32	2.52 $\pm$ 1.75	4
3	115	1.04 $\pm$ 0.52	2.50 $\pm$ 0.72	4
4	5	0.56 $\pm$ 0.04	2.02 $\pm$ 2.33	5
4	20	0.52 $\pm$ 0.07	1.88 $\pm$ 1.90	5
4	40	0.48 $\pm$ 0.08	2.48 $\pm$ 2.45	5
4	55	0.42 $\pm$ 0.03	1.99 $\pm$ 1.40	5
4	80	0.48 $\pm$ 0.06	1.66 $\pm$ 1.95	5
4	114	0.52 $\pm$ 0.10	1.67 $\pm$ 2.41	5
5	5	0.78 $\pm$ 0.14	3.01 $\pm$ 0.88	5
5	12	0.67 $\pm$ 0.05	2.39 $\pm$ 0.58	4
5	24	0.73 $\pm$ 0.29	2.76 $\pm$ 1.37	5
5	42	0.74 $\pm$ 0.22	2.47 $\pm$ 1.65	5
5	60	0.55 $\pm$ 0.05	0.25 $\pm$ 0.37	3
5	70	0.72 $\pm$ 0.12	2.90 $\pm$ 0.14	2
5	80	0.98 $\pm$ 0.51	2.36 $\pm$ 1.57	2
5	90	0.49 $\pm$ 0.04	2.30 $\pm$ 1.0	2
5	100	0.45	-0.77	1

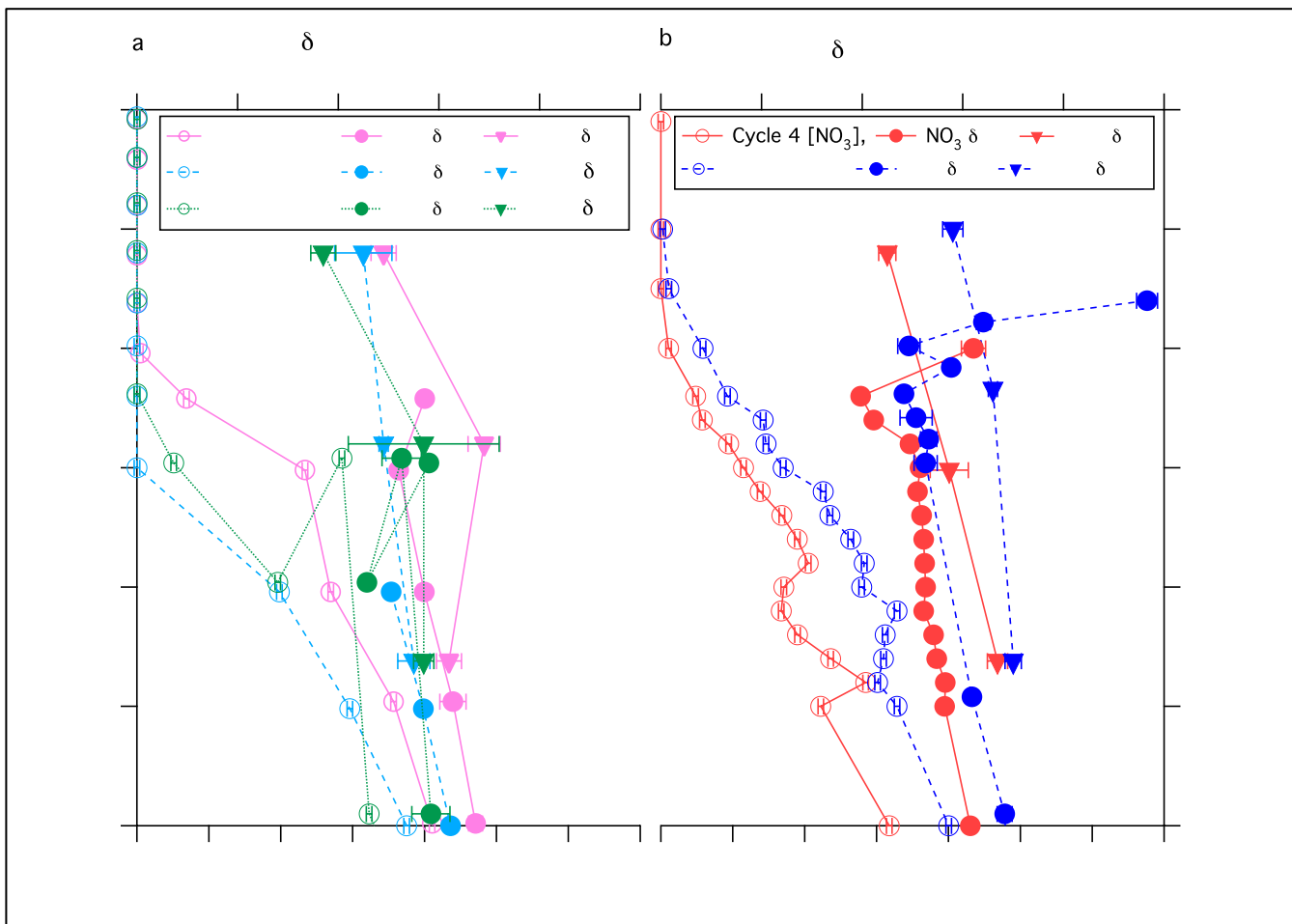
954 **Figures**  
955

956 **Fig. 1**  
957



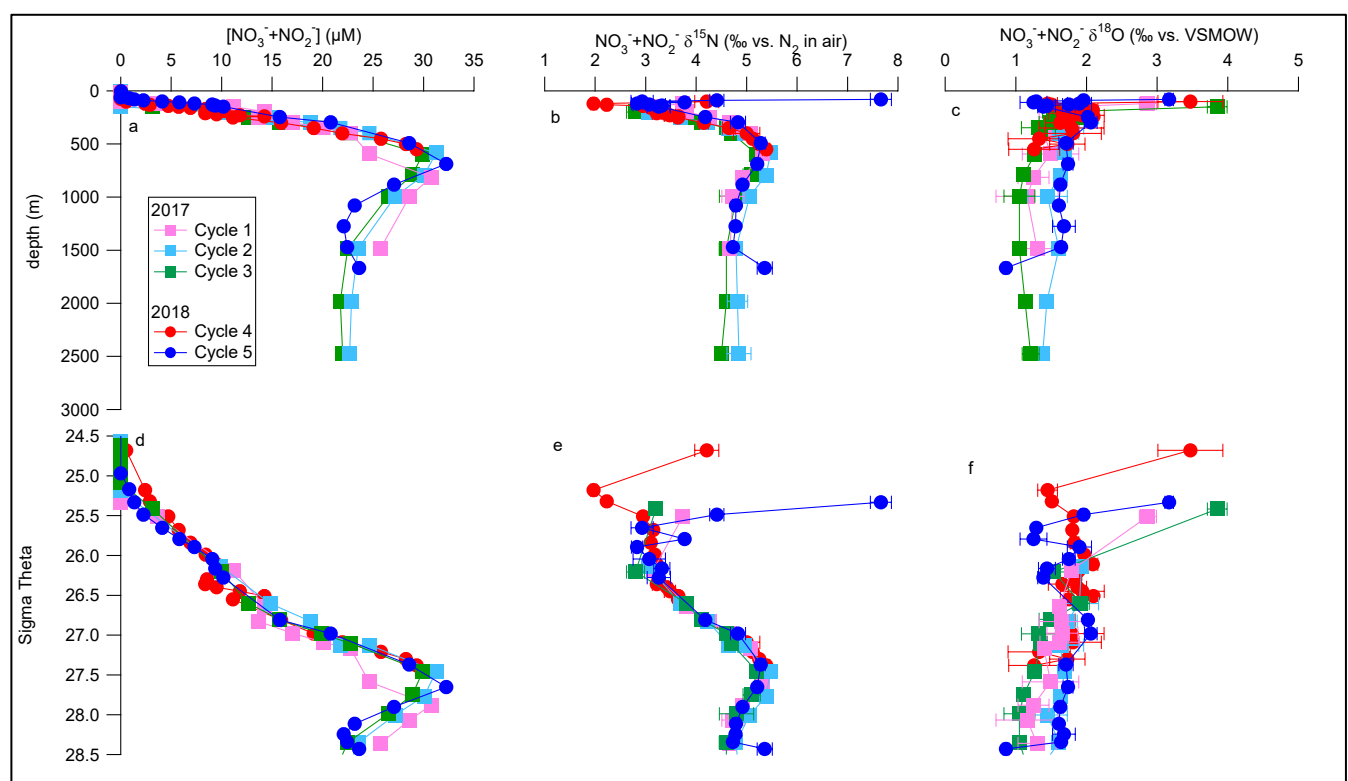
958  
959  
960  
961  
962  
963  
964  
965  
966  
967  
968  
969  
970  
971  
972  
973  
974  
975  
976  
977  
978  
979  
980  
981  
982  
983  
984

**Fig. 2**



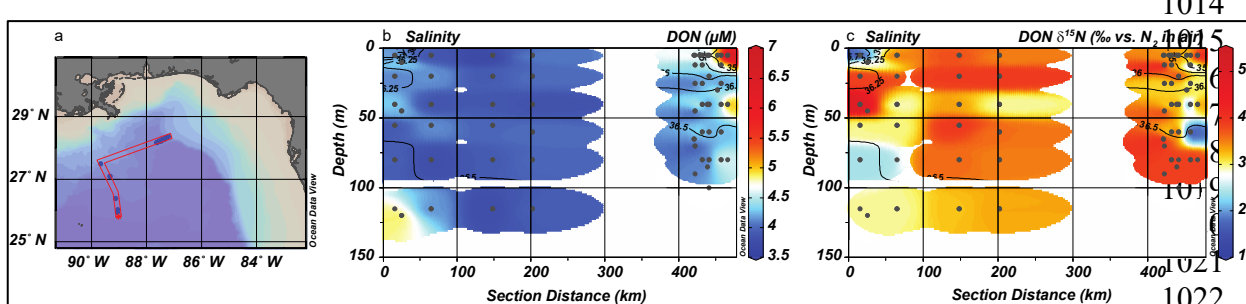
1009  
1010  
1011

**Fig. 3.**



1012

1013

**Figure 4.**

1014

1023

1024

1025

**Fig. 5**

1026

1027

1028

1029

1030

1031

1032

1033

1034

1035

1036

1037

1038

1039

1040

1041

1042

1043

1044

1045

1046

1047

1048

1049

1050

1051

1052

1053

1054

1055

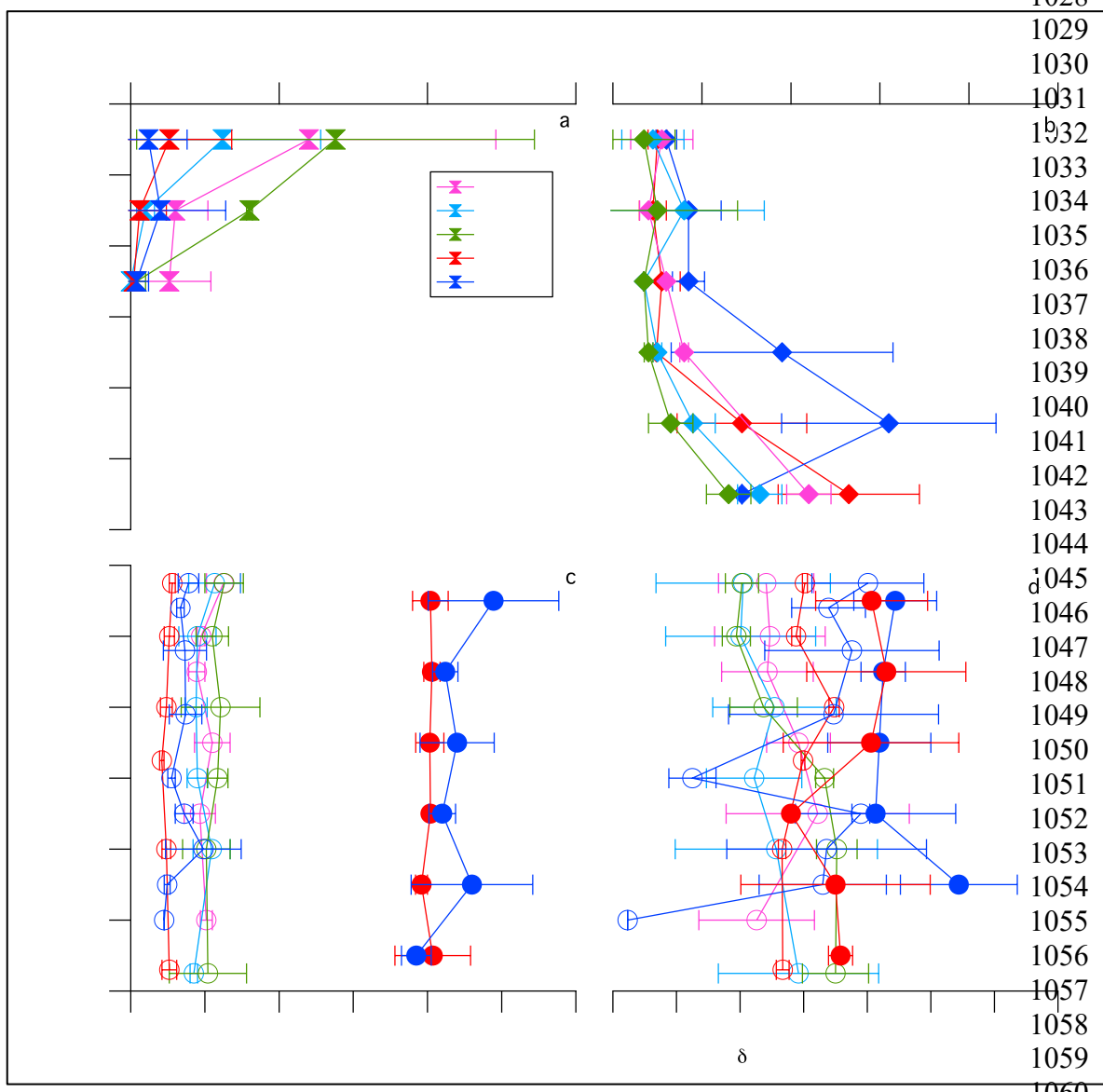
1056

1057

1058

1059

1060



1061

1062  
1063  
1064  
1065  
1066  
1067  
1068 **Fig. 6**  
1069  
1070

